Journal of Structural Geology 164 (2022) 104731

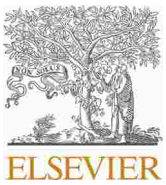

Contents lists available at ScienceDirect

Journal of Structural Geology

journal homepage: www.elsevier.com/locate/jsg

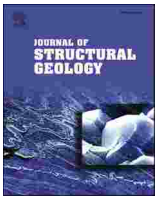

# Lateral and vertical growth and linkage of normal faults in Bozhong8-4 structure of Western Bozhong Sag, Bohai Bay Basin, China☆

Simin Sun [a,b,*], Huayao Zou [a,b], Chengmin Niu [c], Huaiqiang Ren [d,e]

[a] State Key Laboratory of Petroleum Resources and Prospecting, China University of Petroleum (Beijing), Beijing, 102249, China
[b] College of Geosciences, China University of Petroleum (Beijing), Beijing, 102249, China
[c] Tianjin Branch of China National Offshore Oil Company Ltd., Tianjin, 300452, China
[d] Shandong Provincial Key Laboratory of Reservoir Geology, China University of Petroleum (East China), Qingdao, Shandong, 266580, China
[e] Key Laboratory of Deep Oil and Gas, China University of Petroleum (East China), Qingdao, Shandong, 266580, China

ARTICLE INFO

*Keywords:*
Fault growth
Fault linkage
3D segmentation
Dip-linkage
3D growth model
Bohai Bay basin

ABSTRACT

Many previous studies have shown that normal faults are formed by growth and linkage of shorter fault segments through time and have suggested various fault growth models. Although these models have yielded useful information on the evolution of normal fault systems in map view, the three-dimensional (3D) evolution of normal faults is poorly understood. Here, we employ an integrated 3D seismic reflection and well dataset to investigate the 3D growth process of fault zone F1 in the Bozhong 8–4 (BZ8-4) structure of the Western Bozhong Sag (WBS). We i) constructed 3D structural models of individual fault surfaces, ii) calculated the dip angles and dip azimuth distributions on fault surfaces, iii) produced D-d profiles and throw contour maps of fault surfaces, and iv) investigated the 2D/3D segmentation characteristics of geometry and displacement distribution. We found that Fault F1 exhibits segmentation characteristics of geometry and displacement distribution both along strike and dip oriented directions. Vertically, fault surfaces can be divided into three areas (lower, middle and upper parts) that correspond to three stages of regional tectonic evolution (intense faulting, relatively quiescent faulting and post-rifting). The coalescence zone of the upper and lower fault surfaces shows as a sub-horizontal anomaly of geometry and displacement distribution that is sub-parallel to the traces of the horizons. The lower and upper parts of fault surfaces also show segmentation characteristics along strike, which are identified by vertically anomalous zones of geometry and displacement distribution. However, the origins of the segmentation in this case are different. The segmentation of the lower part of the fault developed during the rifting stage is caused by the intersection of faults with different strikes, whereas the upper part of the fault is the result of the lateral growth and linkage of overlapping fault segments. Therefore, not all fault segmentation characteristics along strike can be attributed to fault growth and linkage. Based on 3D fault segment identification, we therefore establish a 3D evolution model of fault zone F1. During the deposition of the Shahejie Fm up to the member (Mbr) 3 of the Dongying Fm in the Paleogene, the faults in this area were highly active, with the development of the NE-trending Fault F1, the NEE-trending Fault Fa and the NW-trending Fault F2. The intersection of Faults Fa and F2 with Fault F1 results in Fault F1 exhibiting segmentation in geometry and displacement distribution. From the deposition of the Mbr 2 of the Dongying Fm, these faults ceased to be active. Since the Pliocene (5.2 Ma), under the influence of transtensional stress field, an en-echelon fault zone was developed in the Neogene strata above fault zone F1 active in the rifting stage. While these faults grow and link laterally, their tip-lines propagate along dip-oriented directions and activate the lower faults and link vertically with them to form the present fault zone F1.

☆ This work was supported by National Major Science and Technology Projects of China: [grant number: 2016ZX05024-003-008].
* Corresponding author. State Key Laboratory of Petroleum Resources and Prospecting, China University of Petroleum (Beijing), Beijing, 102249, China.
*E-mail address:* sun62446@163.com (S. Sun).

https://doi.org/10.1016/j.jsg.2022.104731
Received 27 October 2021; Received in revised form 21 September 2022; Accepted 22 September 2022
Available online 29 September 2022

## 1. Introduction

Normal faults typically consist of overlapping and linked segments along strike in map view (Morley et al., 1990; Peacock and Sanderson, 1994; Anders and Schlische, 1994; Cartwright et al., 1995; Mcleod et al., 2000; Dawers and Underhill, 2000; Su et al., 2011). Abundant studies have shown that large faults are formed by lateral growth and linkage of shorter fault segments (Schlische, 1995; Peacock, 2002; Walsh et al., 2002; Morley, 2002; Kim and Sanderson, 2005). Therefore, the identification of fault segments is vital for the investigation of fault evolution. Conventionally, fault growth is examined by displacement minima of D-d profiles and strike variations of fault trace in plan view to identify the fault segments (Cowie and Scholz, 1992; Willemse, 1997; Schultz and Fossen, 2002; Mansfield and Cartwright, 2001). Early work was mainly focused on the two-dimensional (2D) growth of faults and cannot reveal the three-dimensional (3D) growth characteristics of faults. More recent work has revealed that fault growth is, in fact, the result of 3D propagation and linkage of multiple genetically related fault surfaces with the nucleation points as the initial locations, which include the propagation and linkage of fault surfaces in both horizontal and vertical directions (Mansfield and Cartwright, 1996; Kristensen et al., 2008; Jackson and Rotevatn, 2013; Camanni et al., 2019; Collanega et al., 2019; Torabi et al., 2019; Delogkos et al., 2020; Deng and Mcclay, 2021; Roche et al., 2021). Subsurface fault studies in particular have described anomalous displacement distribution and abrupt variations of geometry in the regions surrounding branch-lines or relay zones along fault strike and dip (Baudon and Cartwright, 2008a; Cohneally et al., 2014; Deng and McClayBilal, 2020). These anomaly zones are often shown as sub-vertical or sub-horizontal zones with higher displacement gradient than the general, or manifested as apparent reductions in dip angles and abrupt variations in fault azimuth on fault surfaces (Marchal et al., 2003; Walsh et al., 2003; Baudon and Cartwright, 2008b; Lohr et al., 2008; Spahic et al., 2013). These provide a basis for the 3D identification of fault segments along both strike and dip directions. Therefore, as long as the coalescence zones of the fault surfaces are identified, we can restore the 3D linkage process of a through-going fault.

Furthermore, normal faults typically strike sub-perpendicular to the extension direction and display an en-echelon or collinear configuration during a single phase of extension (Duffy et al., 2015). The fault evolution in this context generally conforms to the classical fault growth models (Walsh et al., 1999; Trudgill and Cartwright, 1994; Morley, 2002; Childs et al., 2003). However, many multiphase rifts that experience a change in extension direction between stretching phases will typically develop non-colinear normal fault sets (Duffy et al., 2015; Henstra et al., 2015; Deng and McClayBilal, 2020), the intersection between faults with different strikes will also result in the development of vertical anomalies of geometry and displacement distribution on fault surface or high gradients of fault displacement on D-d profiles surrounding the intersection lines (Nixon et al., 2014; Peacock et al., 2017; Roche et al., 2020). It is commonly difficult to distinguish the anomalies from that formed by fault segment linkage; and sometimes they may be wrongly considered as the results of fault propagation and linkage.

The WBS exhibits a high density of normal faults. As one of the major petroliferous structures in the WBS, BZ8-4 structure is controlled mainly by NE-trending Fault F1 and other secondary normal faults with different strikes in its hanging wall ( they are known as fault zone F1 ) . This setting is ideal for this study because previous studies demonstrate the area was subject to two extension events, which resulted in the formation of numerous faults and complex fault interactions with different strikes (Wang et al., 2017; Xu et al., 2018; Zhang et al., 2018). Previous studies considered that the Fault F1 is a continuous fault, did not pay attention to its interaction and genetic relationship with the hanging-wall faults, and ignored the interactions between the faults of two extensional events. Moreover, the relatively shallow burial of the structure and high quality seismic data mean that faults and their intersection or branch lines are well-imaged, and abundant well data allow us to constrain the age of strata adjacent to the faults, and hence constrain the temporal evolution of fault zone F1. In this study we have examined a fault network experienced two-stage extensions by identifying the lateral and vertical segmentation characteristics of faults based on their geometry and displacement distribution in 2D/3D, and improved our understanding of how i) faults with different strikes intersect, resulting in the lateral segmentation of the parent fault during rift stage; ii) lateral growth and linkage of overlapping faults during post-rift stage result in its dip linkage with the fault developed during the rift stage; iii) a large fault evolves by growth and linkage of multiple faults in both lateral and vertical during two-stage extensions. These provide insight into the 3D model of fault growth.

## 2. Geological setting

### 2.1. Regional tectonic evolution

The Bohai Bay Basin (BBB) is located in the eastern China with a total area of approximate 200,000 km$^2$ (Qi and Yang, 2010) (Fig. 1). It is one of the most petroliferous basins in China, accounting for nearly one-third of the total petroleum production of the country (Xu et al., 2014). The BBB has undergone a multi-cycle tectonic evolution, which can be divided into three stages: i) Formation and evolution of crystalline basement of Archean-Early Proterozoic platform (Zhai and Peng, 2007). ii) The formation of cover sequences in stable craton from Middle and Late Proterozoic to Paleozoic when little magmatism and deformation occurred (Meng et al., 2019). iii) Mesozoic-Cenozoic decratonization and continental rift basin development stage. Initial extension in BBB started in the Late Jurassic and continued until the Early Cretaceous. Mesozoic extension is commonly attributed to the Yangtze Plate wedging northwards and the Pacific Plate subducting to the NWN direction. As a result, the NNE-trending Tanlu fault zone (TLFZ) running through the basin underwent left-lateral movement (Zhu et al., 2003; Vergely et al., 2007; Teng et al., 2014) and induced the NW-SE-trending normal faults and corresponding half-grabens. From Late Cretaceous to Paleocene, BBB underwent structural inversion, and the basin was uplifted as a whole, lacking the deposition of this period. Since Eocene, the most intensive extension occurred and produced the BBB, which experienced two stages: the Paleogene rifting and Neogene post-rifting thermal subsidence (He and Wang, 2004). Intense rifting in Paleogene is manifested by marked lithospheric thinning, widespread volcanic eruption and continental rift basins (Fan et al., 2000; Ren et al., 2002; Zhang et al., 2017). It is generally believed that the intracontinental crustal extension caused by the mantle upwelling is the main driving force for the Paleogene rifting (Li et al., 2010).

During the Paleogene, a large number of normal faults occurred and a series of half-grabens controlled by boundary faults were formed under the NW-SE extension. However, due to the influence of pre-existing faults in Mesozoic, these faults trended predominantly NNE and NW/WNW in Bozhong and Jiyang subbasins, and trended NNE and/or NE in the others (Li et al., 2012; Qi and Yang, 2010). According to the distribution of Paleogene formations, the BBB can be divided into 7 subbasins, i.e. Xialiaohe, Bozhong, Huanghua, Jizhong, Linqing, Jiyang and Changwei, and 4 uplifts, i.e. Cangxian, Chengning, Xingheng and Neihuang (Teng et al., 2014)(Fig. 1).

During the Neogene, the BBB has entered the stage of post-rifting thermal subsidence, and the fault activity has been greatly decreased. The whole basin is gradually formed as a unified basin with the subsiding depocenter migrated to the Bozhong subbasin. However, since the Pliocene (5.2 Ma-present), the Neotectonism has brought about the reactivation of the Paleogene normal faults in Bozhong, Jiyang and northern Qikou subbasin and the occurrence of high dense secondary faults in the Neogene strata (Gong, 2004; Teng et al., 2014; Xu et al., 2009; Yu et al., 2011). It is generally believed that the Neotectonic movement is controlled by the right-lateral strike-slip of TLFZ fault zone (Zhu et al., 2003; Suo et al., 2013; Teng et al., 2016).

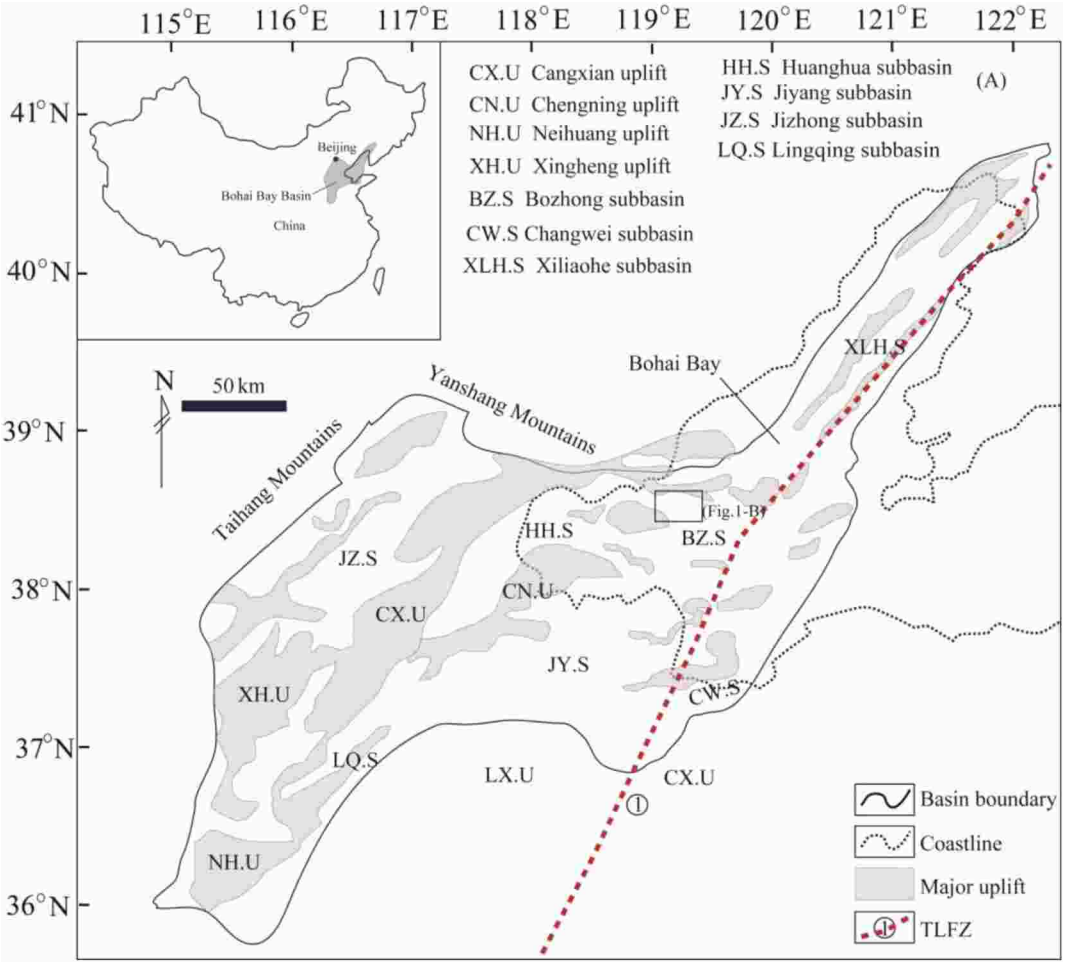


**Fig. 1.** Location of the Bohai Bay Basin, the Tan-Lu fault and subbasins of the Bohai Bay Basin (modified from Teng et al., 2014).

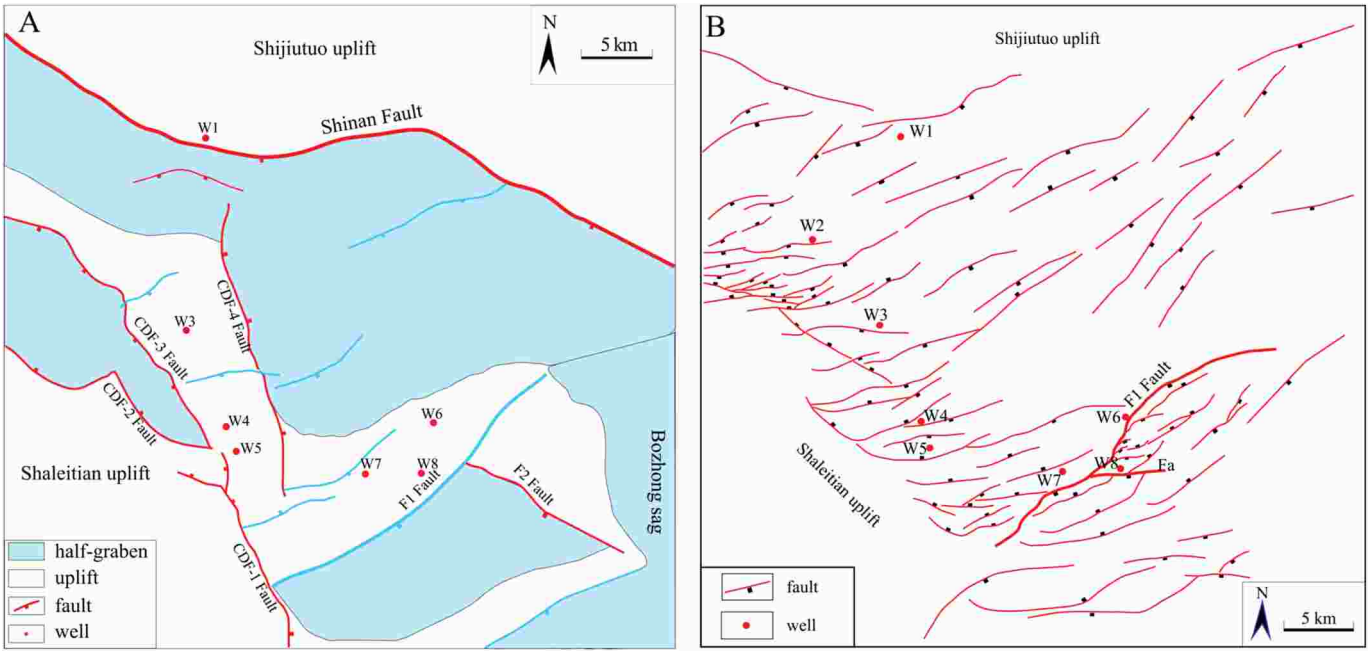


**Fig. 2.** (A) Map (from Horizon T8) showing the structural domains and fault network during the rifting stage in the Western Bozhong sag, including Bozhong8-4 structure. (B) Map (from Horizon T01) showing the fault network during the post-rifting stage in the Western Bozhong sag, including Bozhong8-4 structure. See the box in Fig. 1 for location.

### 2.2. Geological setting of the WBS

The WBS is located in the west of Bozhong subbasin, adjacent to Shijiutuo uplift in the northeast, Shaleitian uplift in the southwest, and Bozhong sag in the southeast (Fig. 2, A). In general, it is sandwiched between Shijiutuo uplift and Shaleitian uplift trending in NW direction, with an area of about 2000 $km^2$. During the rifting stage, it was mainly controlled by the Shinan Fault trending in NW direction. The thickness of the strata is largest near the hanging wall of the Shinan Fault, and pinches out toward the Shaleitian uplift, (Fig. 2, A). There are relatively few faults occurred during this period, and faults primarily strike NW direction, most of which are basement-involved normal faults. Some of the large faults like Fault F1 developed small half-grabens in their hanging wall and uplifts in their footwall respectively. In this way, the area is further divided into three subsidence areas and two uplifts, which determined the main structural framework of the WBS. During the early Neogene, the WBS experienced a period of tectonic quiescence, which displayed relatively smaller extension (He and Wang, 2004). Due to the subsequent Neotectonism (Gong and Wang, 2001; Xu et al., 2009), a large number of smaller faults were produced (Fig. 2, B). These faults strike predominately in NE direction, followed by NW and near EW direction.

Syn-rift strata in this area include Shahejie and Dongying Fm, which has a total thickness of ca. 5000 m (Fig. 3). They are mainly distributed in the sag area, with the maximum thickness near the hanging wall of Shinan Fault, followed by the hanging wall of Fault F1 and F2. The sedimentary environment is dominantly lacustrine-delta facies. Among them, the Mbr 3 and 1 of the Shahejie Fm and the Mbr 3 of the Dongying Fm are thick mudstone dominated by semi-deep or deep lacustrine facies, which are the main source rocks in this area (Du et al., 2016). The post-rift strata include the Neogene Guantao and Minghuazhen Fm and the Quaternary Pingyuan Fm, with a total thickness of 1500–3000 m (Fig. 3). The post-rift sediments were widely distributed in both depressions and uplifts. Guantao Fm is mainly braided fluvial deposits, which is characterized by thick sandstone. It is an excellent reservoir in Neogene of the BBB. The Minghuazhen and Pingyuan Fm were deposited in shallow lacustrine and delta environment, with relatively high shale proportions, and they are the most important seal rocks in the Neogene-Quaternary strata (Hao et al., 2011).

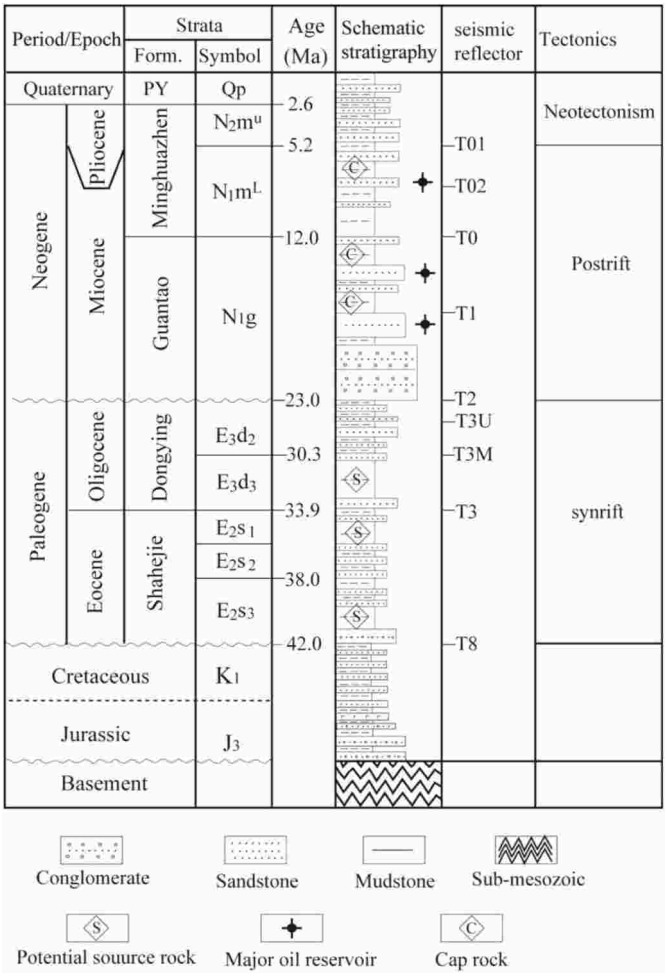


**Fig. 3.** Generalized stratigraphy of the Bohai Bay Basin (modified from Teng et al., 2016). Form. = Formation; PY=Pingyuan.

### 2.3. BZ8-4 structure

BZ8-4 structure is located in the southeastern part of the WBS (Fig. 2). Its northwest is the depocenter of the WBS on the hanging wall of Shinan Fault, which is the largest subsidence unit in the WBS; the southeast is the half-graben controlled by the Fault F1 and F2; its southwest is adjacent to Shaleitian uplift; its northeast is a low uplift. It mainly includes the Fault F1, F2 and other secondary faults and related structures (Fig. 4). It is also the main petroliferous structure discovered in the WBS; the reservoir is sandstones of Guantao and Minghuazhen Fm and the caprock is the intraformational shales interbedded with the reservoir sandstones in Guantao and Minghuazhen Fm.

## 3. Data and methods

The 3D seismic reflection data covering the studying area are provided by the Tianjin branch of China National Offshore Oil Corporation (CNOOC) , its inline and crossline spacing is 25 m and 12.5 m, respectively. The dominant frequency in the Paleogene and Neogene strata is about 35 and 50 Hz. The vertical resolution is approximately 21.4 m and 12.5 m using the average velocity of 2500 m/s and 3000 m/s, respectively.

Through the calibration of drilling stratification and seismic reflection characteristics, nine reflectors are identified and determined, representing the reflections from the Shahejie up to Minghuazhen Fm, respectively, (Fig. 3). After interpretation of the seismic data in terms of faults and horizons, we carried out the time-depth conversion based on Time–Depth velocity data of some key wells, and created a 3D structural model in depth including fault surfaces and stratigraphic interfaces. Subsequently, we calculated the dip and azimuth attributes based on the 3D fault surface model. The attributes of dip, azimuth can highlight corrugations on fault surface. Many previous studies have demonstrated that some corrugations along dip direction originated from lateral linkage of fault segments (Ferrill et al., 1999; Marchal et al., 2003; Lohr et al., 2008; Spahic et al., 2013).

Fault throw is measured by the horizon cut-offs on the footwall and hanging-wall fault surfaces as an approximation of displacement. The displacement distribution on fault surface (Nicol et al., 1996; Childs et al., 2003), the displacement variations along the faults (D–d profiles) (Dawers et al., 1993; Kattenhorn and Pollard, 2001; Kiram et al., 2002) and vertical throw distribution plots (T-z plots) (Ge and Anderson, 2007) were acquired to reveal the kinematics of the faults. We finally carried out the quantitive investigation of fault segmentation, fault growth and linkage by integrating the 3D geometry of fault surfaces and 2D/3D displacement distribution.

## 4. Overview of the BZ8-4 structure fault network

The depth-structure map of horizon T8 best illustrates the geometry of the BZ8-4 structure fault network in the early rifting stage because it is the reflection from the bottom of Shahejie Fm (Fig. 4 A). The structure is dominated by the NE-SW-striking Fault F1 and NW-SE-striking Fault F2 , along with a small amount of shorter faults striking NE or E-W

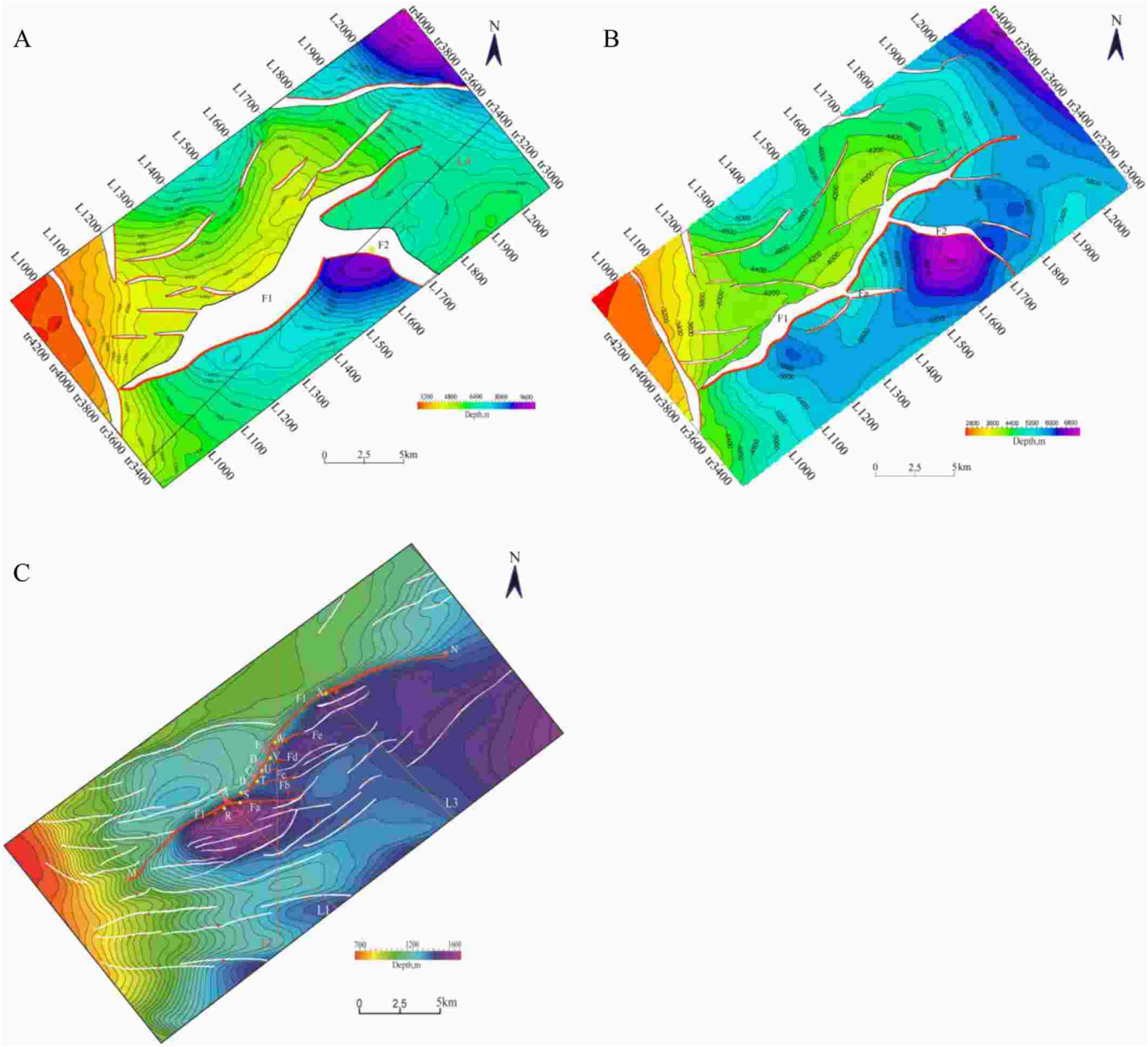


**Fig. 4.** (A) Depth-structure map of bottom of the Shahejie Fm (seismic reflector horizon T8) with key faults labeled; the location of T-z plot on Fault F2 is marked by yellow star. (B) Depth-structure map of bottom of Dongying Fm (seismic reflector horizon T3) with key faults labeled. (C) Depth-structure map of bottom of the Upper Mbr of Minghuazhen Fm (seismic reflector horizon T01) with key faults labeled. The annotation L1000 and tr4200 … etc. represent the inline and cross line number of seismic survey. Seismic lines (Fig. 4) of cross section are indicated. The locations of T-z plots are marked by yellow stars; red stars indicate the locations (labeled by A to E) where hanging-wall faults Fa to Fe intersect with Fault F1 in map view. (For interpretation of the references to colour in this figure legend, the reader is referred to the Web version of this article.)

directions, which are mainly present in the footwall of the Fault F1. Due to the intense activity of Fault F1 and F2, a half-graben is produced in their hanging walls, and the maximum subsiding center is located near the central part of the hanging wall of Fault F2. In the footwall of Fault F1, the uplift was formed due to tiled movement of fault blocks (Fig. 5).

The depth-structure map of horizon T3 best illustrates the geometry of the BZ8-4 structure fault network in the middle stage of rifting because it is located on the boundary between Shahejie and Dongying Fm (Fig. 4 B). Generally, the structural characteristics of horizon T3 are similar to those of the horizon T8. The main difference is that the west segment of Fault F2 changes from nearly E-W-striking to WNW-striking, and the EW-striking Fault Fa in the hanging wall of Fault F1 began to be active.

The depth-structure map of horizon T01 represents the deformation features of Neotectonism during the post-rift stage (Fig. 4 C). The structural characteristics of BZ8-4 in this stage are quite different to those in rifting stage. The number of faults increased markedly, primarily striking in NE or NEE. In plan view, the length of Fault F1 is more than 25 km, and five NEE to NE-trending branch faults, Fault Fa to Fe, occur in the hanging wall of the central part of the Fault F1. They splay from Fault F1, forming a “broom” like fault system.

Fig. 6 shows the 3D spatial relationship of faults in the fault zone F1. It can be seen that the Fault F1 intersects with Fault F2 and Fault Fa to Fe at different angles in 3D. Among them, the Fault F2 is nearly perpendicular to the Fault F1, intersecting with the Fault F1 in the deep. Fault Fa intersects with Fault F1 at an acute angle. Fault Fb, Fc, Fd and Fe are

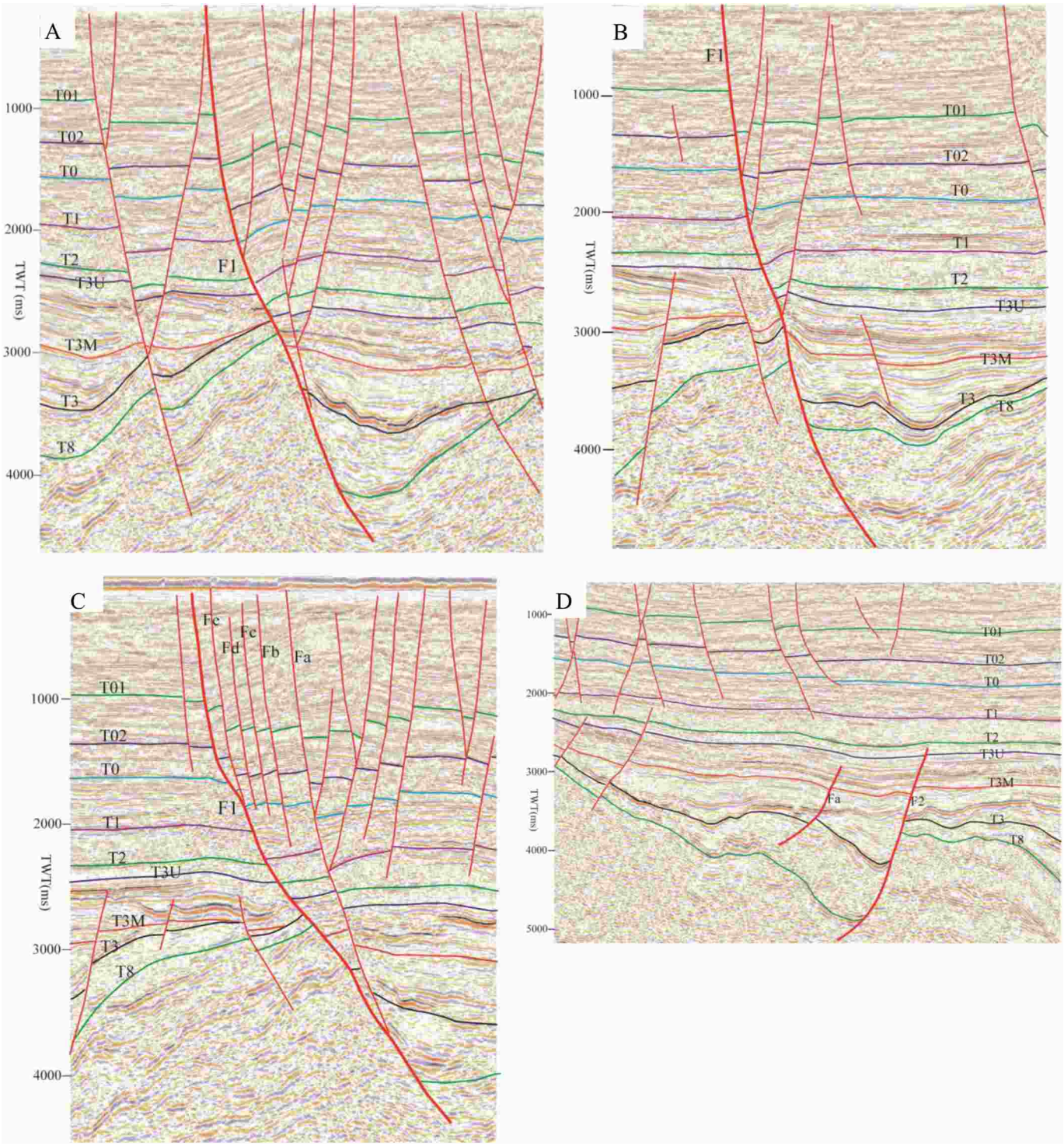


**Fig. 5.** (A to C) interpreted seismic profiles L1-L3 through the Bz8-4 structure showing the dipping characteristics of the fault zone F1; (D) interpreted seismic line L4 parallel to the F1 fault. (for locations, see Fig. 4); TWT = two-way travel time.

smaller in scale and intersect with the upper part surface of Fault F1 at acute angles, showing a stepped-like geometry on dip-oriented cross-section (Fig. 5 B). It can be seen from the seismic section and fault surfaces in 3D that the faults in this area can be obviously divided into two sets of fault systems (Fig. 5), the upper and the lower, with horizon T2 as the boundary. In addition to the Fault F1 and Fa, the lower fault system, including Fault F2, disappears upward below the horizon T2; whereas the upper fault system only occurs in the Neogene strata.

Fault F1 is a basement-rooted normal fault with the upper tip typically located in uppermost Neogene strata (close to the seafloor). Its fault surface appears to be composed of two listric "sub-segments", the location of vertical linkage is located near horizon T2, showing significant vertical segmentation (Fig. 5A and C). The strata of Shahejie and Dongying Fm thicken toward the fault surfaces of Fault F1 and F2 in the hanging wall. On the contrary, the strata thickness decreases towards the fault surface in the footwall. T-z plots, taken at a range of locations along Fault F1 (Fig. 7), show that fault throws decrease rapidly from horizon T8 up to T3M (Fig. 7A, B). Fault Fa also displays the feature

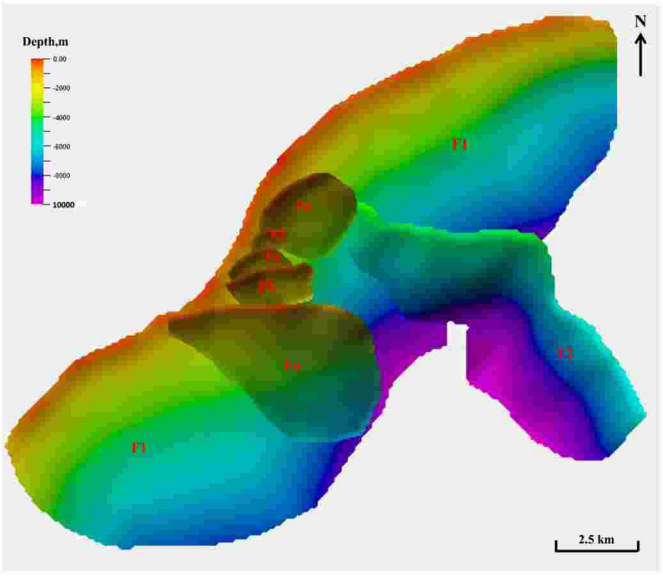


**Fig. 6.** 3D fault surface models of Fault F1 and related hanging-wall faults.

similar to that of Fault F1 (Fig. 7D). These indicate Fault F1 and Fa were syn-sedimentary faults during this phase. In contrast, T-z plots from the Mbr 2 of Dongying Fm (between horizon T3M-T2) display a relatively tabular geometry and show little variation in throw with depth, suggesting that this phase was the period of faulting quiescence (Ge and Anderson, 2007; Duffy et al., 2015). Fault F2 is also a basement-involved fault, with the upper tip typically located in uppermost Paleogene strata (Fig. 5D). Its fault throw decreases gradually from horizon T8 up to the upper horizons on T-z plots and disappears in the Mbr 2 of Dongying Fm, indicating its reduced activity (Fig. 7C). It is clear that Fault F1, F2 and Fa show an evolution from syn-sedimentary faulting to quiescence during the Paleogene. This indicates that the fault activity of the Paleogene rift stage in studying area can be further divided into two phases, the intense faulting phase from the deposition of Shahejie Fm up to the Mbr 3 of Dongying Fm and the relatively quiescent phase from the deposition of the Mbr 2 of Dongying Fm.

The Paleogene regional stress field in BBB is characterized by NW-SE extension (Qi and Yang, 2010; Teng et al., 2014). It is clear that the NE-trending Fault F1 and the NW-trending Fault F2 were synchronously active under this stress field during the Paleogene, (Fig. 2. A). The strike of Fault F1 is perpendicular to the regional extension direction, which can be considered as a direct response to the Paleogene extension. Although the strike of Fault F2 is almost consistent with the regional extension direction, it still shows the characteristics of syn-sedimentary

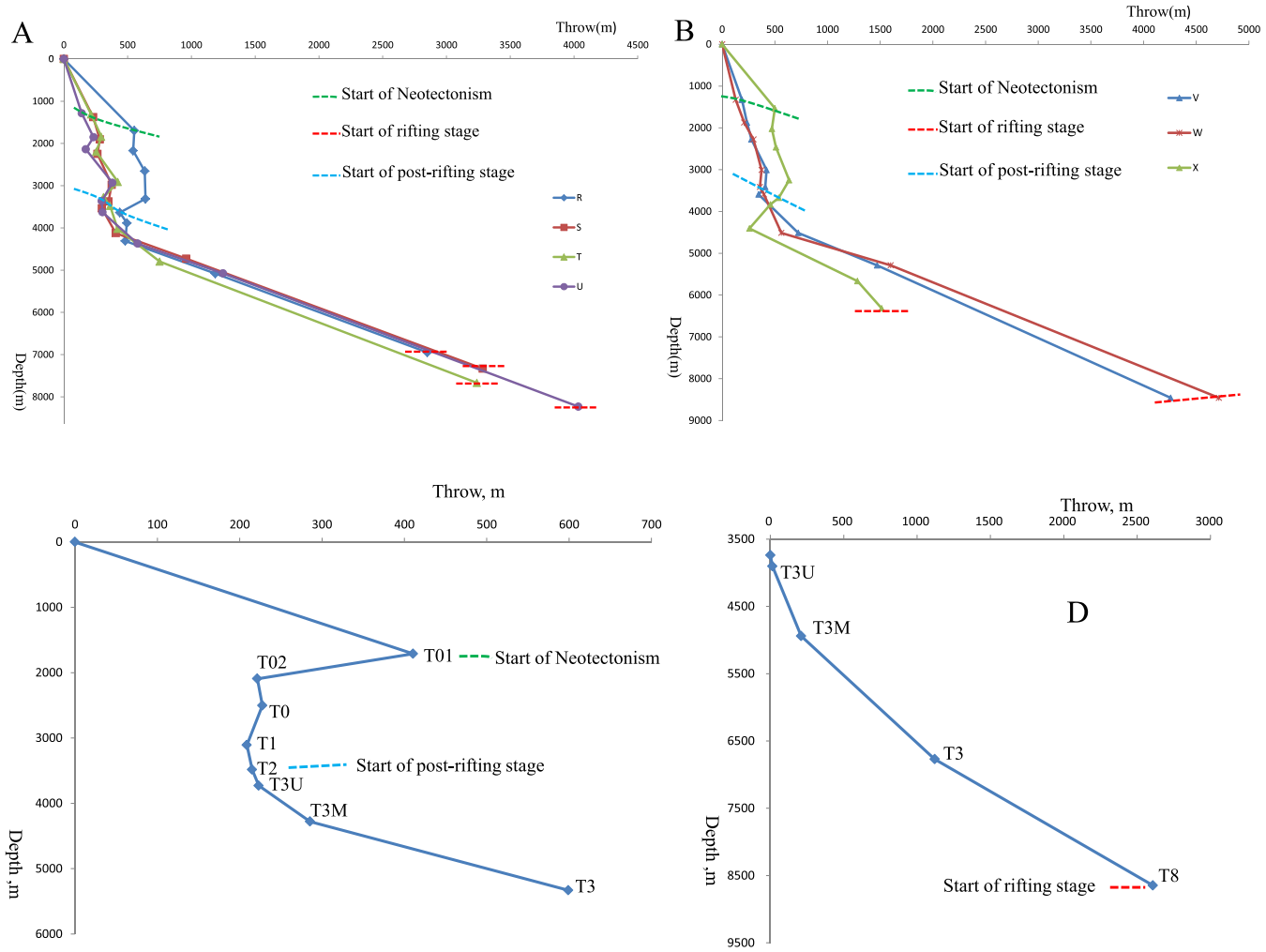


**Fig. 7.** (A and B) T-z plots taken at various locations along the Fault F1, C and D at F2 and Fa. Note that the locations of the plots are marked by stars on Fig. 4. A and C. These plots provide evidence that the Fault F1 and Fa was intensively active during $E_2s$ and $E_3d_3$ of the rifting stage; reactivated during post-rift stage, especially during Neotectonic period; and kept in quiescent between the two faulting stages; the Fault F2 was active only during the rifting stage, (see text for more details).

faults. In fact, in addition to Fault F2, Shinan Fault, the boundary fault of WBS, also trended in NW during Paleogene (Fig. 2. A). On a larger scale, most of master faults trended NW/WNW and NE in Bozhong and Jiyang subbasins, but had NE and/or NNE strikes in the others in BBB. The NW/WNW-trending orientations are considered to be inherited from the Mesozoic tectonic framework of this area (Hou et al., 2001; Qi and Yang, 2010; Li et al., 2012). This indicates the orientations of normal faults are controlled not only by Cenozoic stress field, but also by the orientations of pre-existing Mesozoic basement fault assemblages in this area. Similar fault networks have also been observed in other areas (Morley et al., 2004; Henza et al., 2011; Phillips et al., 2016, 2019).

In the Neogene, T-z plots from Fault F1 display an asymmetric “C" geometry (Fig. 7A, B), skewed toward the lower tip, with throw maxima on T-z plots located near the horizon T1. However, the throw variations are relatively small between horizon T2 and T01, which suggests relatively weak faulting activity; whereas the gradients of throw variations above the horizon T01 increase significantly, which is typically interpreted to indicate the surface-rupturing faults (Baudon and Cartwright, 2008c). The apex of “C" geometry on T-z plots is commonly interpreted to represent the nucleation sites (Barnett et al., 1987; Ge and Anderson, 2007). We therefore can interpret the faulting evolution of the Neogene as follows: Faulting activity in the Neogene initiated as blind faults at or before horizon T01, and subsequently propagated to free surface and turned to syn-sedimentary faults during the phase of Neotectonism (Fig. 3.).

In conclusion, the faulting evolution in studying area can be divided into two stages: the rift and post-rift stages. The former can be further divided into two phases, the intense faulting from the deposition of Shahejie Fm up to Mbr 3 of Dongying Fm and the tectonic quiescence phase from the deposition of the Mbr 2 of Dongying Fm. The latter can be divided into two phases, the relative tectonic quiescence period of the deposition of Guantao Fm up to the Lower member of the Minghuazhen Fm and the relative intense faulting period from the deposition of the Upper member to present (the phase of Neotectonism).

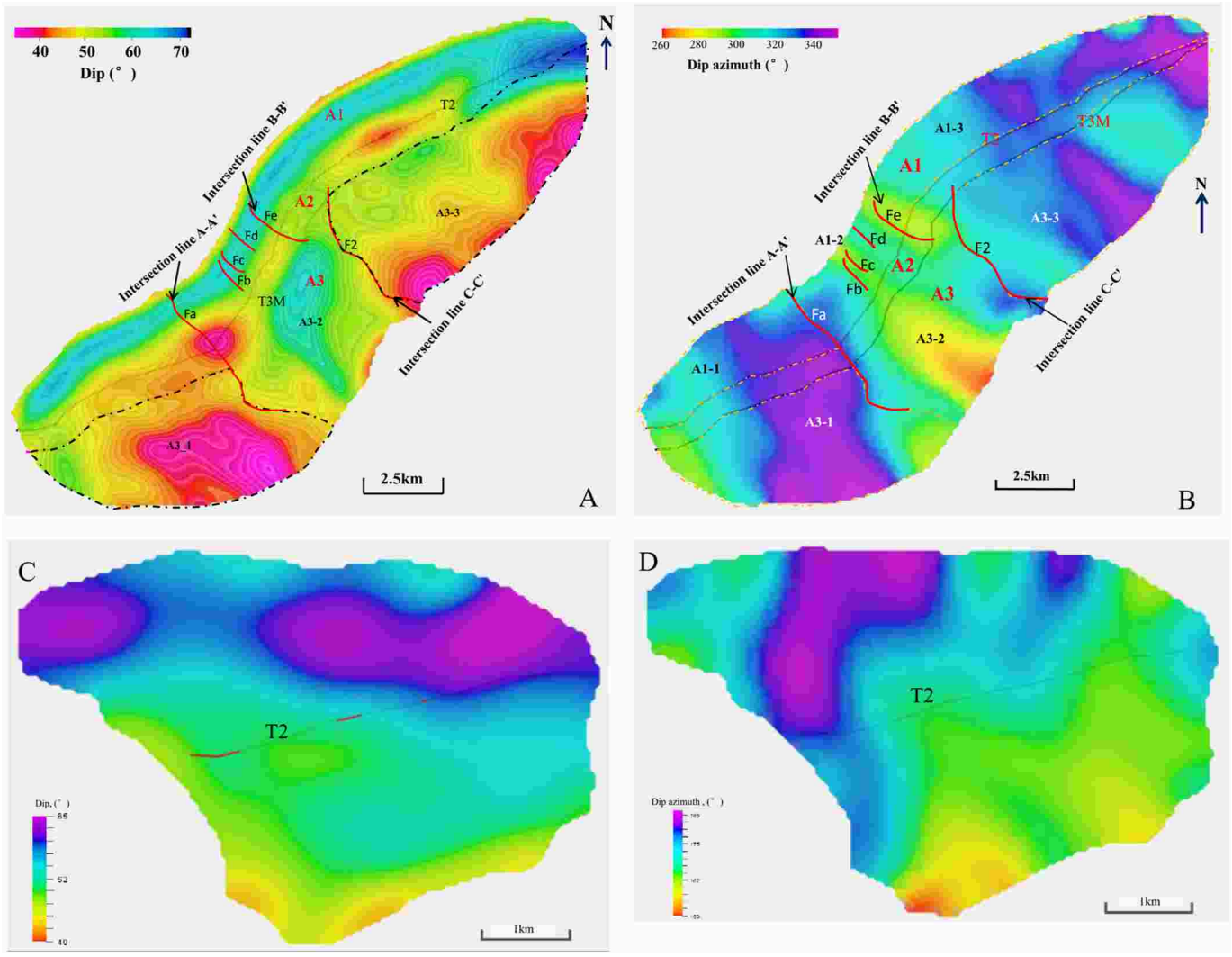


**Fig. 8.** Fault surface attribute maps of (A) dip angles, and (B) dipping azimuth of Fault F1. Projected fault cut-offs of key seismic stratigraphic horizons are shown with solid lines marking hanging-wall cut-offs; red solid lines perpendicular to cut-off lines marking the intersection or branch lines of Fault F1 with other hanging-wall faults. Dotted lines marking the lateral segment areas of different faulting stages of Fault F1. (A) dip attribute distribution in degree showing vertical segmentation of Fault F1 surface at the T2 and T3M cut-offs as the boundaries, they are A1, A2 and A3 areas; and A3 can been further divided into three sub-areas along strike by intersection lines. (B) Dip azimuth attribute distribution in degree showing lateral segmentation of Fault F1 surface at the intersection lines of A-Á, B-B´and C-C´ as the boundaries. (C) Dip angles and (D) dipping azimuth of Fault Fa. Projected fault cut-off of horizon T2 is shown with solid line marking hanging-wall cut-off. Attribute maps illustrating the apparent variation across the horizon T2 cut-off, (see text for more details). (For interpretation of the references to colour in this figure legend, the reader is referred to the Web version of this article.)

## 5. Geometry and throw distribution of fault zone F1

### 5.1. Geometry of fault surfaces

On the surface of Fault F1, the dip angles range from 35° to 70° (Fig. 8A). Dip variations divided the fault surface into three areas in vertical. Area A1 is distributed above Horizon T2, ranging from ca. 50°–70°. Area A2 is distributed between horizon T2 and T3M, ranging from ca. 40°–50°; and Area A3 is distributed below the horizon T3M, ranging from ca. 35°–60°. The dip values of Area A1 are larger with little variation along strike. Area A2 displays as a narrow anomalous zone with relatively small dip angles located between horizon T2 and T3M. Whereas the dip values in Area A3 are small with great variations along strike. Taking the intersection lines of A-Á and C-C′ as the boundary, the Area A3 can be divided into three distinct sub-areas along strike ( the A3-1, A3-2 and A3-3 ) . Among them, the dip values of the A3-2 are the largest, generally greater than 55°. The second is the A3-3, and the A3-1 has the smallest mean dip angle, generally less than 50°.

The dip azimuths mainly show great lateral variations (Fig. 8B). The intersection lines of A-Á, B-B′ and B-C′ divide the fault surface of Fault F1 into three sub-areas along strike. As a result, according to the characteristics of dip angle and dip azimuth, the surface of Fault F1 can be divided into three areas along the dip direction, the Area A1, A2 and A3; the Area A1 and A3 can be further subdivided into three sub-areas along their strikes.

The dip angles and azimuths on the surface of Fault Fa exhibit apparent variation across the horizon T2 (Fig. 9), and can been divided into two parts vertically, which suggests that the two parts experienced different types of faulting evolutions.

It is clear that dip azimuths of the fault surface exhibit significant lateral segmentation, and the abrupt variation zones of dip azimuths are consistent with the position of vertical branch lines or intersection lines. This indicates that they may represent the connecting lines of the laterally overlapped fault surfaces. In addition to area A3, dip attributes mainly show vertical segmentation, reflecting the result of fault dip-linkage. Area A2 can be interpreted as the breached relay zone between vertical overlapping segments, which is equivalent to the horizontal branch lines between vertically linked fault surfaces.

For the cause of these phenomena, we make the following explanations. It is generally believed that a fault can be segmented in 3D (vertically and horizontally), both containing corresponding relay zones leading to complex fault geometries (Peacock and Sanderson, 1991; Childs et al., 1996; Camanni et al., 2019; Roche et al., 2021). Lateral overlapping faults produce horizontal relay zones, and breached relay zones result in lateral linkage of fault segments and formation of through-going faults (Anders and Schlische, 1994; Cartwright et al., 1995; Walsh et al. 1999; Frankowicz and McClay, 2010; Fossen and Rotevatn, 2016), therefore result in abrupt variations of fault strike surrounding vertical connecting lines (branch lines) between fault surfaces (Fig. 9A). For vertically overlapped faults, relay zones were developed between overlapping segments, breached relay zones result in the vertical linkage of segments (Childs et al., 1995; Deng and Mcclay, 2021; Roche et al, 2021), and vertical through-going faults may demonstrate relatively low dips along connecting faults or horizontal branch lines between fault surfaces (Fig. 9B) (Peacock and Zhang, 1994; Peacock, 2002; Cohneally et al., 2014; Rotevatn and Jackson, 2014; Roche et al., 2020).

### 5.2. Characteristics of throw distribution

For a more unequivocal investigation of fault zone F1, we measured the throw of nine horizons (from horizon T8 up to T01) in milliseconds TWT and converted them to depth in meter by time-depth conversion data acquired from the wells. The results are plotted in two ways: the D-d profiles in 2D that illustrate the displacement variations of each horizon along strike and the displacement contours that demonstrate the displacement distribution in 3D on fault surfaces.

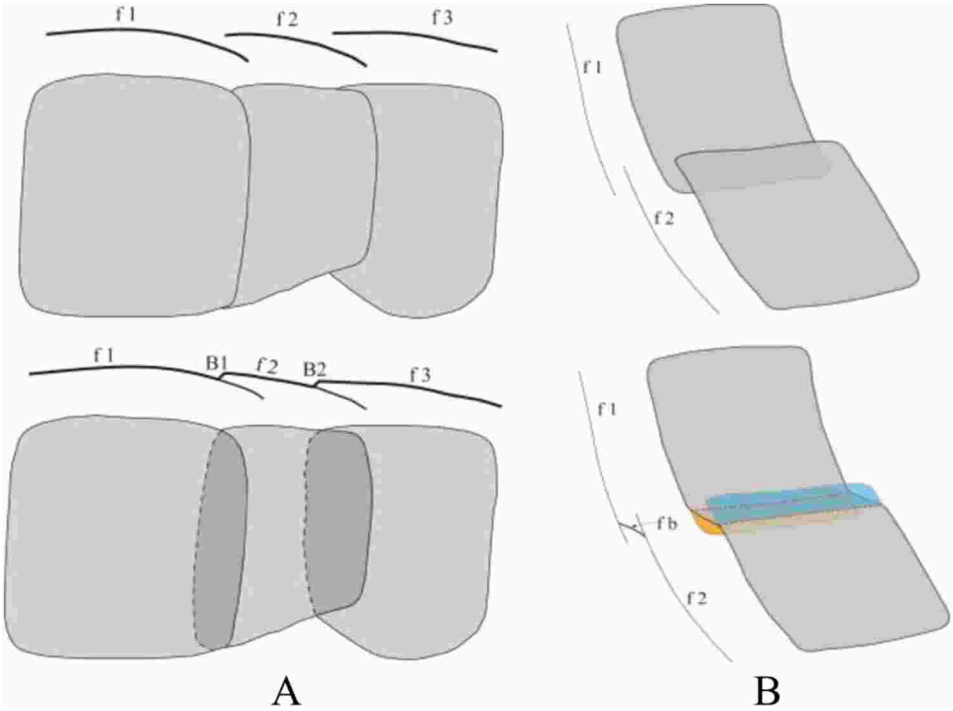


**Fig. 9.** Schematic map patterns showing development of propagation and linkage of laterally and vertically overlapped normal faults. Dotted lines indicating vertical and horizontal branch lines, respectively. (A) Lateral fault linkage produces vertical branch line and associated strike variations surrounding the branch lines; (B) fault dip linkage produces horizontal branch line and associated dip reduction surrounding the branch line.

### 5.2.1. Throw on D-d profiles

*5.2.1.1. Fault F1.* The throw variations of the nine horizons along Fault F1 from T8 up to T01 are shown on D–d profiles (Fig. 10). The throw on horizon T8 is largest with the maximum throw of 4796 m, and decreases rapidly upward, with throw maximum 533 m at horizon T3U; and then, increases gradually upward and attains the maximum of more than 700 m at horizon T0 and T1. On the other hand, throw presents great variations along fault strike, displaying multiple maxima and minima, which are normally used to infer the centers and tips of individual fault segments that have linked to form a single through-going fault (Childs et al., 1995; Su et al., 2011; Frankowicz and McClay ,2010; Sun et al., 2016). Specifically, on the horizon T8 (Fig. 10, A), throw is largest near the central segment and decreases toward its two tips, but there is a large step at the intersection line C-C′ (intersection with NW-SE-striking Fault F2). The throw curve of horizon T3 can be divided into three segments by two throw steps at the intersection line A-Á (intersection with Fault Fa) and C-C′ (intersection with Fault F2) (Fig. 10. A). These are consitent with the characteristics of fault segmentatiuon along strike on geometry of fault surface (Area A3). From the horizon T3M to T01, the throw profiles seem to have similar curves (Fig. 10. B, C). Taking the throw maxma A and E as the boundaries (intersection line A-Áand B-B′), the Fault F1 is divided into three segments along strike, the segment MA, AE and EN (see also Fig. 4, C), which correspond to the sub-area A1-1, A1-2 and A1-3 on fault surface (Fig. 8, B). Specifically, from horizon T2 to T01, the throw curve of segment EN shows roughly V-shaped geometry, which is similar to that of typical, isolated normal faults. The segment MA displays the left half branch of V-shaped geometry; the segment AE is composed of multiple left half of V-shaped geometry separated by throw minima. This feature is most typical on horizon T01 and T02 on which there are four distinct throw minima, separating the displacement curve into four sub-units. The four throw minima in segment AE correspond to points A, C, D and E on the structure map (Fig. 4, C), which are also the sites of intersection of Fault Fa, Fc, Fd and Fe with Fault F1 respectively. The sharp throw decrease of Fault F1 at the location B corresponds to the intersection between Fault Fb and F1. It is clear that the throw variations of Fault F1 along strike are highly controlled by the development of hanging-wall faults, which indicates the possible genetic relationship between them.

*5.2.1.2. Faults Fa to Fe.* It can be seen from throw curves of the Fault Fa to Fe that they are highly similar (Fig. 11. A to E), the throws on these faults are largest near the Fault F1 and decrease away from it, displaying a geometry of the right half of the typical “V"-shaped geometry. Among them, on the throw curves of horizon T02 and T01, the throw maxima on Fault Fa and Fe are very close to that on Fault F1 at other side of intersection lines. The throw maxima of the Fault Fb, Fc and Fd is less than that on Fault F1 at other side of intersection lines due to their overlapping. When their throws on overlapping segments are added up, they present much better correspondence with the throw maximum on the left half branch on Fault F1 (Fig. 11F.).

It is clear that for the throw curves of Fa to Fe, if joining them together with their overlapping segment pairs of Fault F1 on the other side of the intersection lines, they can merge to form a relatively complete “V" shaped geometry. Throw curves on these overlapping fault segment pairs are complementary and display higher throw gradients in the region overlap, e.g. Fa with segment AB of Fault F1; the sum throw of Fa to Fd with segment BE of Fault F1; Fe with the southern segment of EN of Fault F1 (Fig. 11 F). These characteristics are believed to be due to displacement transfer between overlapping segment pairs. The transfer

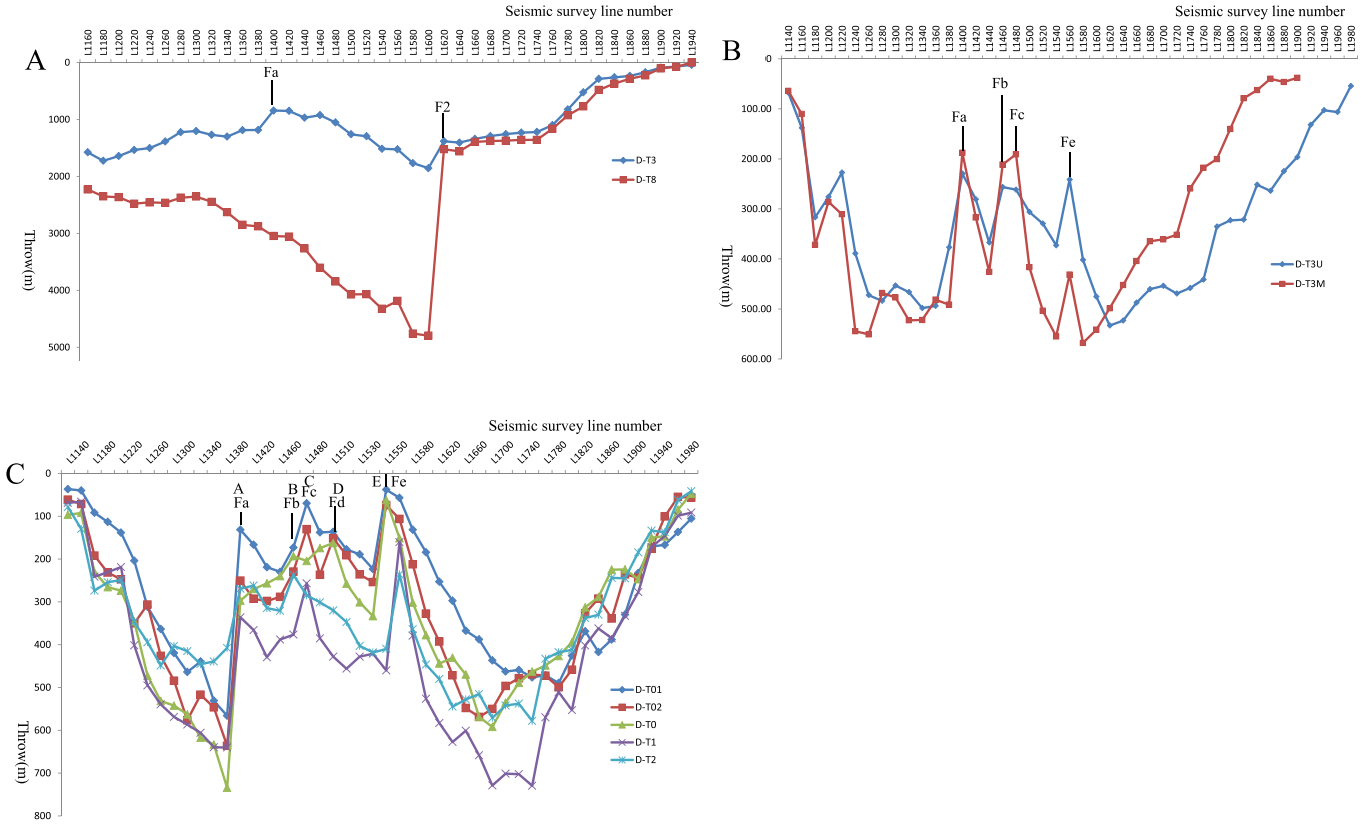


**Fig. 10.** (A) Along-strike throw profiles of Fault F1 for the horizon T8, T3. The profile indicating the abrupt throw variation and minimum are consistent with the intersections of Fault F1 with F2 and Fault Fa. (B) Along-strike throw profiles of Fault F1 for the horizon T3M, T3U. The profiles indicating the throw minima are consistent with the intersections of Fault F1 with the faults Fa, Fb, Fc, and Fe. (C) Along-strike throw profile of Fault F1 for the horizons T2, T1, T0, T02 and T01, respectively. The profiles indicating the throw minima are consistent with the intersections of Fault F1 with the faults Fa to Fe (see text for more details).

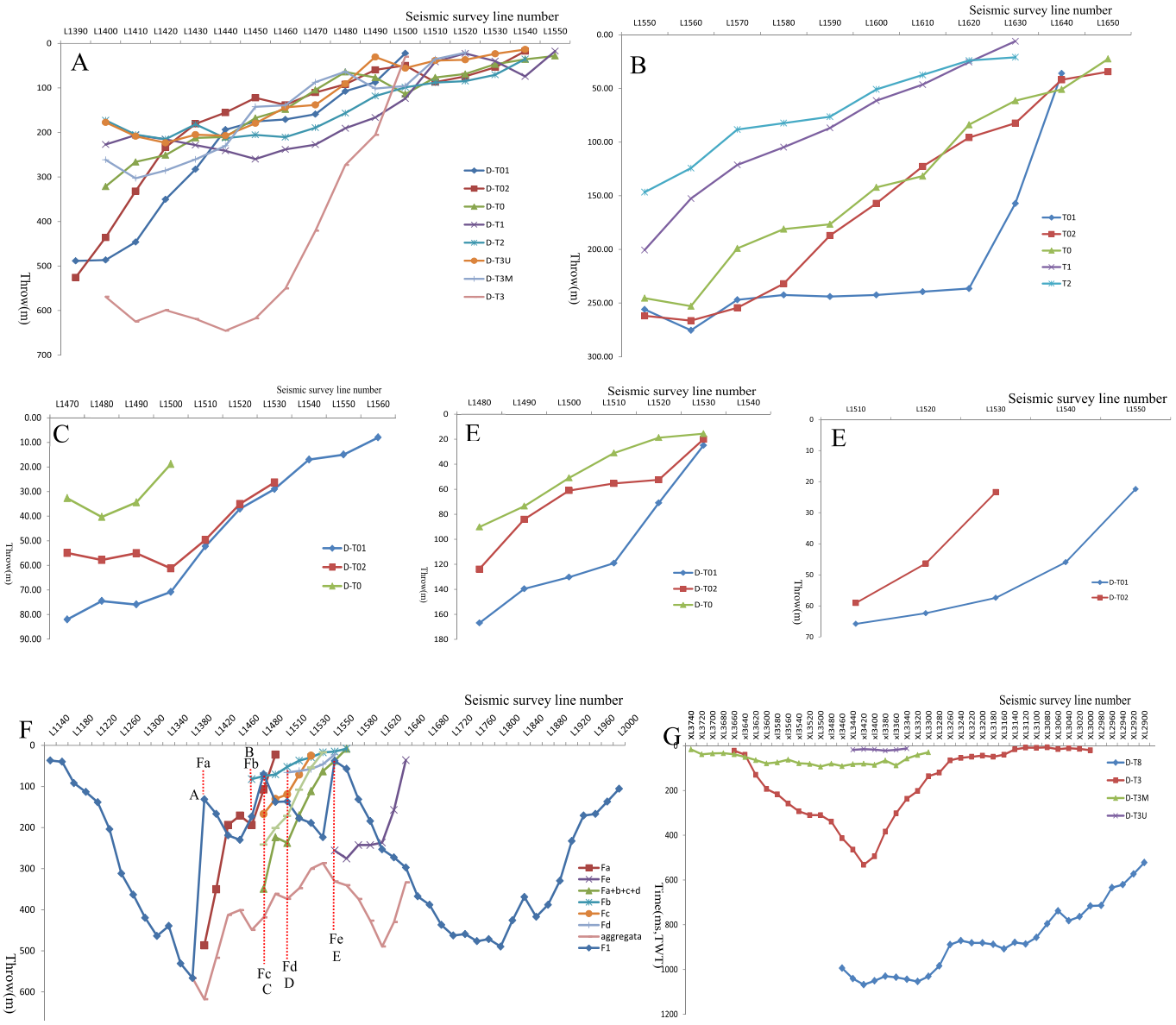


**Fig. 11.** (A) Along-strike throw profiles of Fault Fa for the horizon T3, up to T01, respectively. (B) Along-strike throw profiles of Fault Fb for the horizon T0, T02 and T01. (B) and (C) Along-strike throw profiles of Fault Fb and Fc for the horizon T0, T02 and T01. (D) Along-strike throw profiles of Fault Fd for the horizon T02 and T01. (E) Along-strike throw profiles of Fault Fe for the horizon T2 up to T01, respectively. (F) Along-strike throw profiles of the faults F1 and Fa to Fe for the horizon T01, respectively. The throw minima on Fault F1 indicating the branch lines with hanging wall faults Fa to Fe; Fa + b + c + d mean the sum throws of overlapped Fa to Fd along their strikes; aggregate means the sum throw of overlapping segments of F1 network. The throw curves of the five faults Fa to Fe are symmetrical to that of Fault F1 on the left side of the branch lines, forming the full "V"-shaped geometries; (G) Along-strike throw profiles of Fault F2 for the horizon T8, up to T3U, respectively. (see text for more details).

of displacement from one segment to another occurs through relay zones (Peacock and Sanderson, 1991; Cartwright et al., 1995). This indicates that Fault F1 network were originally an overlapping fault array with relay zones developed between overlapping segment pairs, and subsequent linkage of faults result in the breaching of relay zones and formation of the present through-going Fault F1 and branch faults Fa to Fe. The present intersection lines between Fault F1 and faults Fa to Fe are, in fact, vertical branch lines connecting laterally overlapped segments (Walsh et al., 1999; Cohneally et al., 2014; Camanni et al., 2019). Ideal throw profiles on overlapping fault typically provide an aggregate throw profile which is similar to that of an single fault (Barnett et al., 1987; Peacock and Sanderson, 1991; Baudon and Cartwright, 2008b). In studying area, however, the aggregate throw exhibits signifcant displacement deficits (Fig. 11. F) , this may be attribute to: i ) present Fault F1 is still in the displacement accumulation period of the early stage of fault linkage; ii) displacements or strains between the overlapping fault segments are taken up by numerous subsidiary faults and other deformation structures (Childs et al., 1993, 1995; Peacock and Sanderson, 1994).

*5.2.1.3. Fault F2.* The throw of horizon T8 up to T3U along the Fault F2 are plotted in Fig. 11 G. The Fault F2 has a throw maximum ca.2771 and 1271 m on horizons T8 and T3, respectively, and decreases rapidly upward, and so do the fault length. It kept active during most of the Paleogene period with the maximum displacement occurred nearly at the same location. Fault F2 displays an asymmetrical displacement profile being skewed to the northwest direction during its dominated faulting phase. This indicates its interaction with the Fault F1 in northwest orientation.

### 5.2.2. Throw distributions on fault surfaces

*5.2.2.1. Fault F1.* Displacement distribution on 3D fault surface is a another useful tool for fault growth investigation in recent years. Many geologists have shown that different types of normal faults have their own distinct displacement distribution patterns on fault surface (Mansfield and Cartwright, 1996; Childs et al., 2003; Duffy et al., 2015; Torabi et al., 2019). Barnett et al. (1987) assumed that the displacement distribution on surface of ideal, isolated blind faults is characterized by elliptical contours concentric about a centrally located maximum displacement. Many studies have also revealed that different types of normal faults and interaction between neihbouring faults will result in distinct displacement contour patterns on 3D fault surfaces (Chapman and Meneilly, 1990; Childs et al., 1993, 2003; Nicol et al., 1996; Baudon and Cartwright, 2008a). As a result, the displacement contours on fault surface can be used to identify different types of faults or fault segments and to examine the fault growth and linkage. Therefore, we acquired the throw contour maps on the fault surfaces of fault zone F1 by cut-off measurement of nine horizons (Fig. 12A and B). Vertically, Fault F1 surface can be divided into three distinct areas with the boundaries of horizon T3M and T2, which is consistent with that on geometrical fault surface. The throw contours below the horizon T3M are approximately parallel to the traces of horizon T8 or T3 and decrease uniformly upward, and display lateral segmentation controlled by Fault F2 and Fa (Fig. 12 A). Whereas the area between horizon T3M and T2 (Area A2) is mainly composed of multiple elliptical contours, which are characterized by centering on throw minima. Above the horizon T2, the great throw variations of Area A1 along strike illustrate lateral segmentation characteristics of Fault F1 (Fig. 12 B). The Area A1 can be subdivided into three sub-areas by the branch lines of A-Áand B-B´. Among them, the mean throw of sub-area A1-2 is relatively small. The throw of the sub-area A1-1 and A1-3 is relatively larger. The shape of throw contours in the sub-area A1-3 are fully elliptical with the throw maximum at the center of the ellipse. The long axes of ellipses are distributed along the traces of horizon T1 or T0. Howerer, the geometry of throw contours in the sub-area A1-1 presents the left semi-elliptical with the throw contours terminated abruptly at the branch line with Fault Fa. Similar contour geometry also occurs on left side of intersection line with Fault

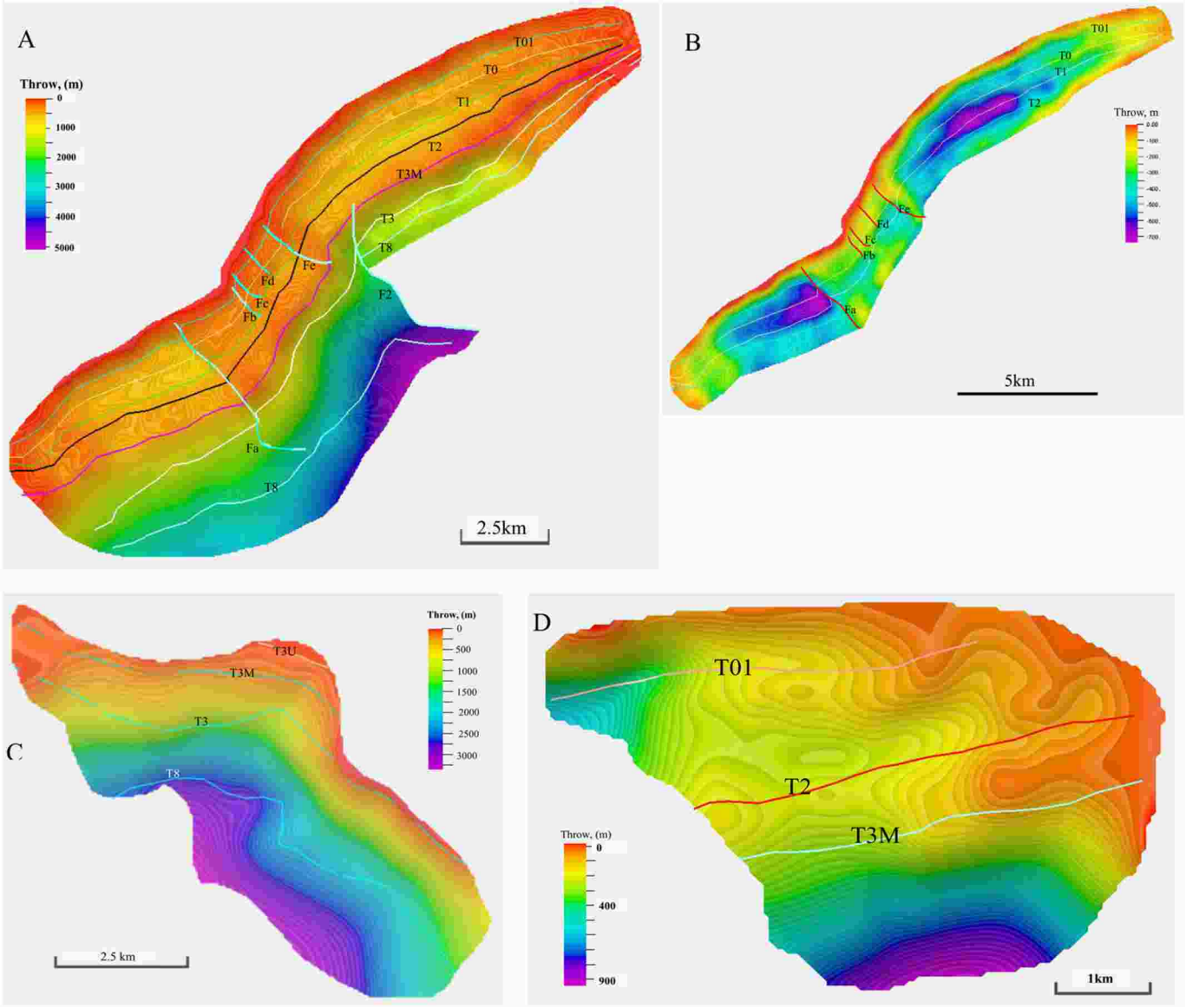


**Fig. 12.** Throw distributions map of fault surfaces of Fault F1 and Fa to Fe. Projected fault cut-offs of horizon T8 up to T01 are shown with solid line marking hanging-wall cut-offs; solid lines perpendicular to fault strike marking the intersection or branch lines with hanging-wall faults. (A) Fault F1; (B) upper part of F1 above horizon T2; (C) F2; (D) Fa; (E) Fb; (F) Fc; (G) Fd; (H) Fe.

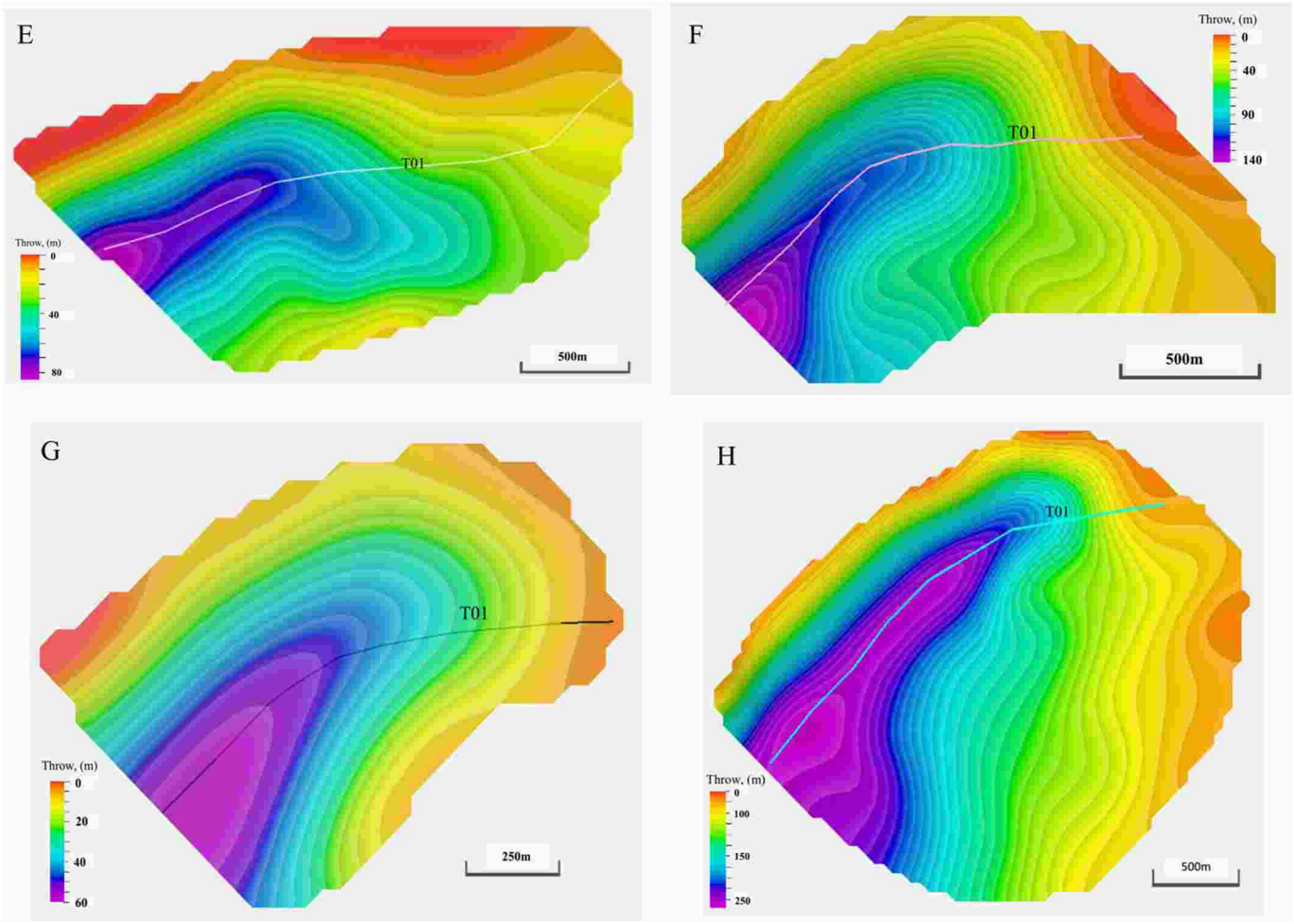


**Fig. 12.** (*continued*).

Fe in the sub-area A1-2. It is clear that these lateral segmentation caused by kinematics are consistent with that by fault surface geometry.

*5.2.2.2. Fault F2.* Vertically, the throw distribution on the surface of Fault F2 can be divided into two distinct areas with the boundary of horizon T3 (Fig. 12 C). The throw contours below horizon T3 are sub-parallel to the traces of horizon T8 or T3 and decrease uniformly upward; whereas the area above horizon T3 displays such features that most of throw contours decrease upward and cross obliquely to the horizons traces between horizons T3 to T3U except for the central part segment, indicating a progressive decrease in the fault length (Childs et al., 2003).

*5.2.2.3. Faults Fa to Fe.* The throw distribution on the surface of Fault Fa is similar to that of Fault F1 (Fig. 12 D). It is also divided into three areas vertically with horizon T3M and T2 as boundaries. In the area below the horizon T3M, the throw contours are nearly parallel to the trace of horizon T3 and decrease upward. The throws between horizon T3M and T2 are smallest. Whereas in the area above the horizon T2, the throw contours present geometry of the right semi-ellipse. The throw contours below the horizon T01 are oblique to the trace of horizon T01, whereas the throw contours above horizon T01 is parallel to the trace of horizon T01, and the throw gradient increases significantly. Compared with Fault Fa, the height of fault surfaces of Fault Fb, Fc, Fd and Fe is significantly reduced, and their fault suefaces are mainly distributed in Neogene strata above horizon T2. Their throw contours on fault surface present the crudely semi-elliptical geometry with maxima at branch lines and long axes approxiately located at the horizon T01 (Fig. 12 E to H). It is clear that throw contours on both sides of the fault intersection lines are symmetrical in the Neogene; If they are spliced together, they merge to form fully-elliptical geometry, which blind normal faults typical have.

*5.2.2.4. Throw contour patterns on fault surfaces.* Based on above analysis of throw distribution on fault surfaces, we have concluded four types of displacement contour patterns on fault surfaces in studying areas (Fig. 13). i) Type I: the parallel or sub-parallel pattern. Throw contours are approximately parallel to the horizon traces and decrease uniformly upward which are primarily distributed on the lower part of fault surfaces below horizon T3M and above horizon T01. It is normally interpreted as syn-sedimentary faults (Childs et al., 2003; Baudon and Cartwright, 2008a). ii ) Type II: the positive elliptical contour pattern. It has a throw contour pattern in which contours of equal throw form concentric ellipses centered on the point of throw maximum with the longer axis of the ellipse parallel to the horizon traces, and it is typically be interpreted as the isolated, blind normal faults, the throw maximum represents the initial fault nucleation (Barnett et al., 1987; Walsh and Watterson, 1987; Nicol et al., 1996; Baudon and Cartwright, 2008b). iii ) Type III; negative elliptical contour pattern. Its throw countour feature is similar to that of Pattern II expect for throw minimum located on its certer. This pattern is previously unreported. In this area, it represents the quiescence periods of faulting activity, and is used as the identification marks for the dip linkage of vertically segmented faults. iv ) Type IV: Semi-elliptical pattern. The contour pattern of fault

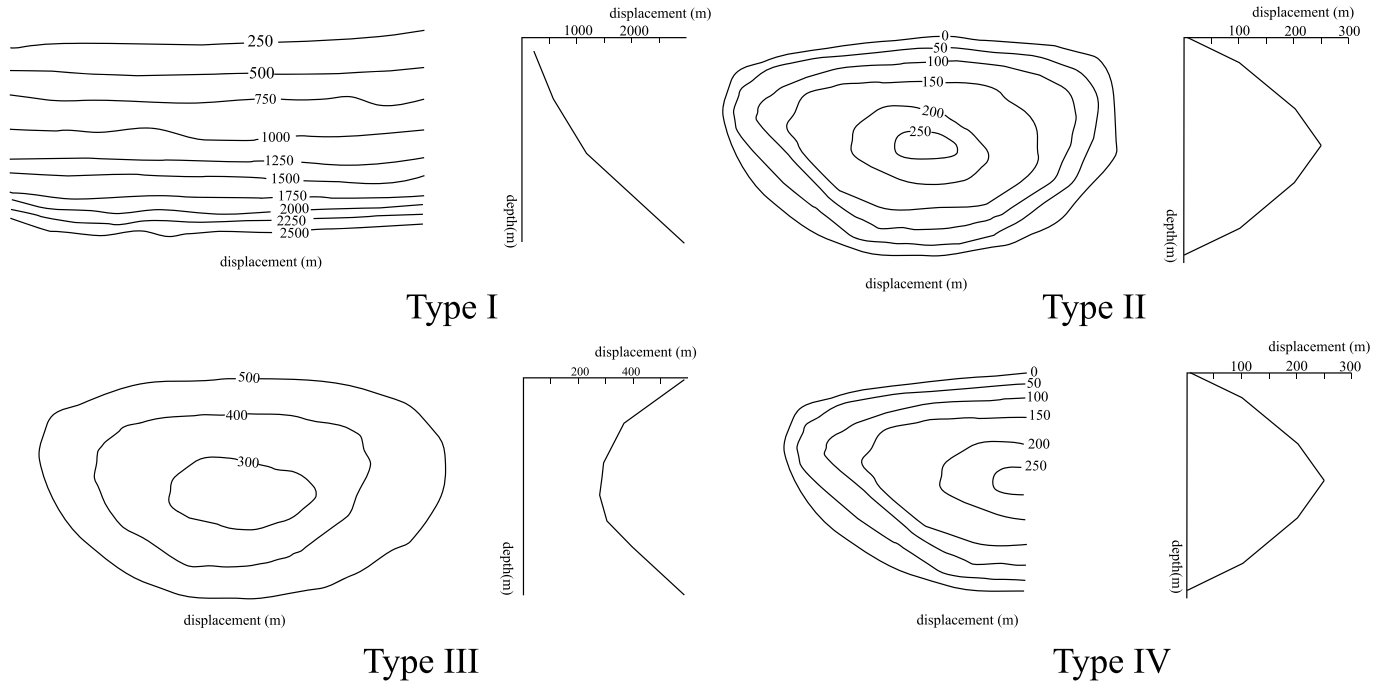


**Fig. 13.** Schematic map showing throw contour patterns on fault surfaces and corresponding typical T-z geometry.

displacement is equivalent to the left or right half of pattern II (Figs. 13 and 14). In studying area, most of them can be interpreted as an original elliptical fault surfaces be cut into two parts along the vertical axes.

## 6. Fault segmentation and interaction styles

### 6.1. Lateral and vertical segmentation characteristics of fault F1

From the above presented geometric and kinematic characteristics of Fault F1, it can be seen that the Fault F1 displays segmentation characteristics in both vertical and horizontal directions. Vertically, bounded by horizon T3M and T2, the fault surface of Fault F1 can be divided into three different areas (A1, A2, A3), each shows its own distinctive geometry and kinematics. Laterally, the three areas can been further subdivided into three sub-areas along their strikes. The segmentation characteristics of the area A3 are controlled by Fault F2 and Fa. The area A1 and A2 are controlled by the Fault Fa and Fe.

### 6.2. Fault intersecting styles during the paleogene

As presented above, the lateral segmentation of Fault F1 is controlled by its hanging-wall faults. However, the interaction styles between them are notably different in two faulting stages. During the deposition of Shahejie Fm up to Mbr 3 of the Dongying Fm, as an intense rifting phase in studying area, the NE-SW-trending Fault F1 was initially active under the NW-SE extensional stress and the NW-SE-trending Fault F2 also

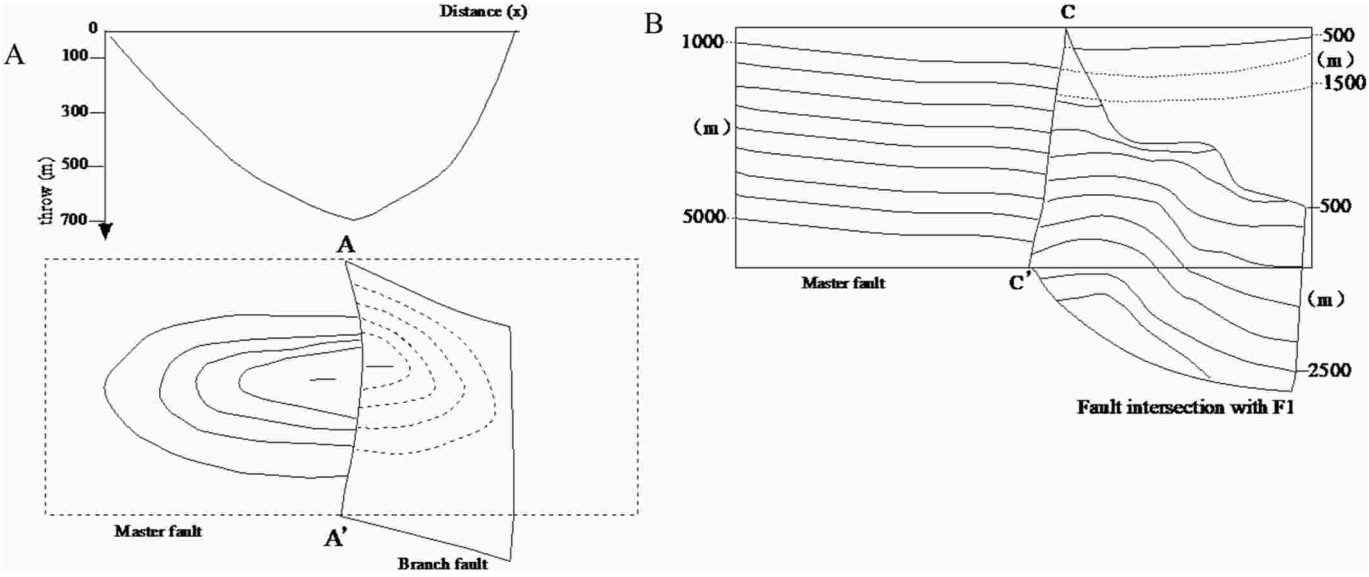


**Fig. 14.** Schematic map showing two types of fault interaction. (A) Fault linkage style, including displacement contour pattern and corresponding typical geometry of D-d profiles on both sides of branch line; (B) fault intersection style, indicating interactions on both sides of intersection line between intersected faults with different strikes.

began to be active as the pre-existing fault in Mesozoic (Zhang et al., 2018; Meng et al., 2019). The Fault F2 has asymmetrical throw profiles being skewed to the northwest on horizon T8 and T3, with the throw maximum on horizon T8 located near the surface of Fault F1 (Figs. 11 G, Fig.12 C). Displacement distribution pattern on fault surface is characterized by Type I. This suggests that Fault F2 nucleated near the Fault F1, retarded by Fault F1 in northwest direction and terminated against it during lateral propagation. The Fault Fa was active later than Fault F2 because it did not displace the horizon T8. It has the throw maximum on horizon T3, which is located near the surface of Fault F1 (Figs. 11 A, Fig.12 D). This also suggests that the fault nucleated near the surface of Fault F1 and intersected with Fault F1 westward, and propagated eastward. Although the intersection of Fault Fa and F2 with F1 resulted in the lateral segmentation of Fault F1 in geometry and kinematics in the Paleogene, but Fault F1 is not the result of fault segment growth and linkage, because the throw distribution of Fault Fa and F2 are not related to that of Fault F1 on other side of the intersection lines in corresponding period (Fig. 14 B). Their interaction styles are consistent to the intersecting modes (Watterson et al., 1998; Maerten et al., 1999) or the abutting interaction styles (Duffy et al., 2015), and are obviously different from which caused by segment growth and linkage of typical overlapping faults (Childs et al., 1993; Duffy et al., 2015).

### 6.3. Fault growth and linkage style during the Neogene

During the Neogene period, the Fault F1 intersected with the hanging-wall faults at an acute angle (Fig. 4C). The throw distribution of Fault Fa to Fe is closely related to that of the Fault F1 on other side of the branch-lines, specifically, on both sides of the branch-lines, i) the fault traces can form a arc-shaped geometry on horizon T01 structure map (Fig. 4C). ii) throw curves on D-d profiles can also form a full V-shaped geometry (Figs. 10 and 11). iii) The geometry of throw contours can form a full ellipse (Fig. 12). These characteristics typically reflect the geometry and displacement distribution of an isolated, blind normal fault, indicating that the segment Ma and Fault Fa, segment AB and Fault Fb, segment BC and Fault Fc, segment CD and Fault Fd, segment DE and

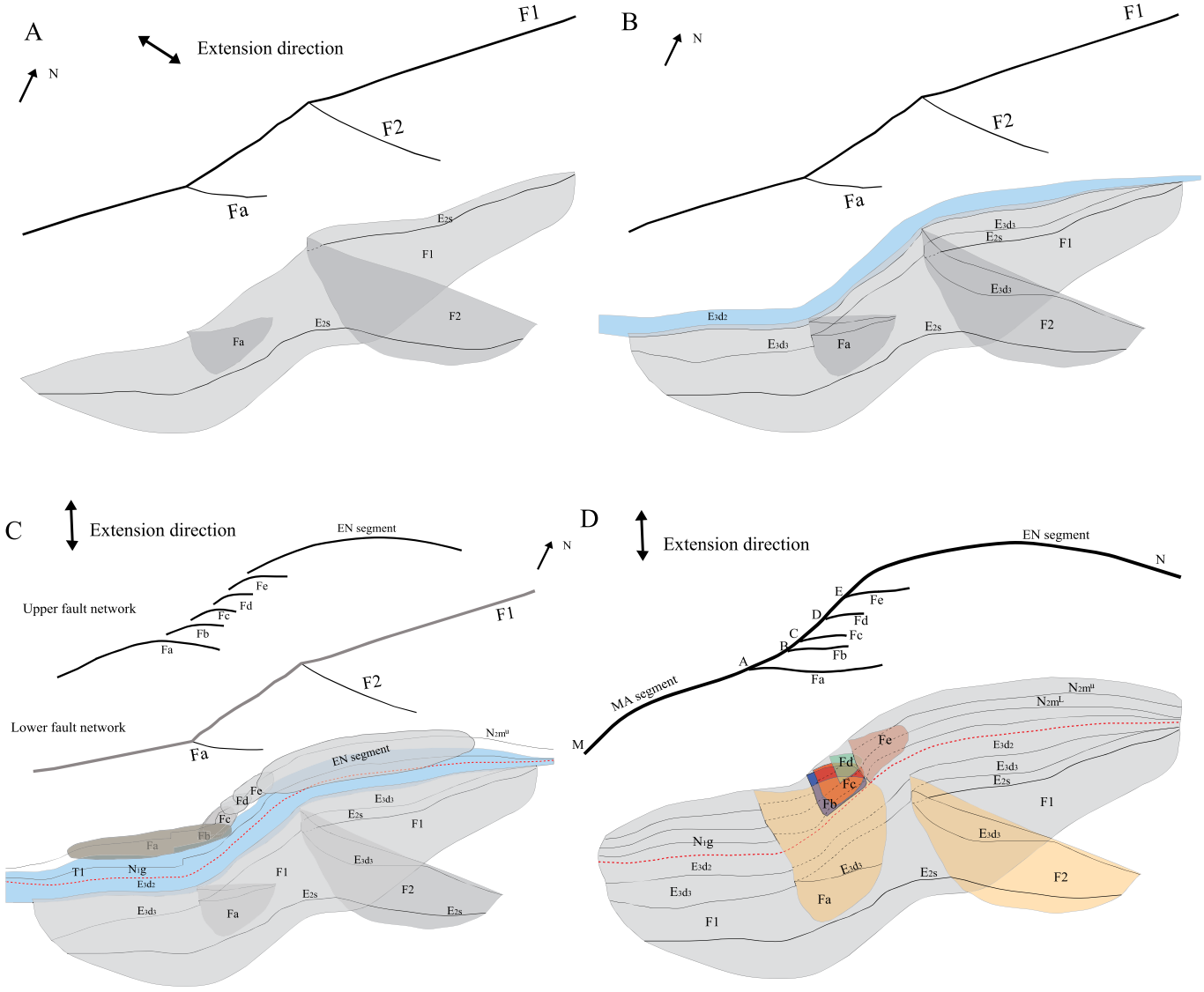


**Fig. 15.** Evolution schematic map of growth and linkage of the fault zone F1 in 3D. (A) Development of fault intersection of different faults during the deposition of Shahejie Fm up to the Mbr 3 of Dongying Fm ($E_2s$-$E_3d$); Fault F1, F2 and Fa were active as syn-sedimentary faults. (B) The quiescent phase of fault zone F1 as buried faults during the deposition of the Mbr 2 of Dongying Fm ($E_2d_2$), the blue indicates deposition of tectonic quiescence. (C) Development of en-echelon faults consisting six faults during the Neotectonism phase, which were distributed in Neogene strata. The lower and the upper fault surfaces did not link vertically. (D) The present-day F1 fault zone. Solid lines on fault surfaces indicating the stratigraphy interfaces and the red dash line represents the interface of the Paleogene and Neogene. (For interpretation of the references to colour in this figure legend, the reader is referred to the Web version of this article.)

Fault Fe and segment EN were originally active as an isolated fault. Their subsequent lateral propagation, overlap and linkage formed the present Fault F1 network, with their northeastern parts of segments degraded to the hanging-wall branch faults of Fault F1 (Fig. 14 A). Therefore, these fault interactions are consistent with the previous studies on the "propagation, interaction and linkage of normal faults". It is clear that the interaction styles of the upper and lower parts of Fault F1 with the hanging-wall faults are remarkedly different. Therefore, fault intersection and fault growth and linkage of can both result in the fault segmentation in geometry and kinematics.

## 7. Evolution of the fault zone F1

The aim of this section is to integrate the geometrical and kinematic data presented in this article, to constrain the evolution of fault zone F1. Based on the above analysis, we can infer the evolution process of fault zone F1 as follows.

During the deposition of Shahejie Fm up to Mbr 3 of Dongying Fm (between horizon T8-T3M), under the NW-SE extensional stress in the early Paleogene (Yu et al., 2011), the Fault F1 and F2 in studying area began to be active, and subsequently, the Fault Fa also began to be active. The Fault F2 and Fa intersected with Fault F1. Fault F1 is divided three segments due to the intersection with them (Fig. 15 A). From the deposition of the Mbr 2 of Dongying Fm (between T3M and T2), the Fault F1, F2 and Fa progressively ceased to be active, and their fault surfaces were buried by the strata of Mbr 2 of Dongying Fm (Fig. 15 B).

In the Neogene, the throw maxima are mainly distributed along the horizon T1 (segments AE and EN) or between horizons T1 and T0 (segment MA), displaying the elliptical geometry on surface of Fault F1 and C-shaped throw distribution on T-z plots (Fig. 7), which typically represent the blind fault activity. Whereas above the horizon T01, throw contours display the Type I pattern on the surface of Fault F1, and a significant change occurs in the throw gradient of the T-z plots. The apex of C-shaped displacement distributions and the center of a ellipse typically represent the nucleation site of a blind normal fault (Barnett et al., 1987; Nicol et al., 1996); the Type I displacement pattern and abrupt throw gradient normally indicate the transition of faulting activity from blind normal faults to syn-sedimentary faults (Childs et al., 2003). This indicates that the faults initiated within areas of maximum throw values and turned into syn-sedimentary growth from horizon T01 during Neogene. However, timing of the blind stage is commonly difficult because the nucleation site cannot represent the time of faulting. Generally, nucleation might be more reasonably expected to occur at depth than at free surface (Baudon and Cartwright, 2008c). So we can infer that the blind faults may initiated between horizon T0 to T01 above the buried Fault F1 (corresponding to the deposition of Lower member of Minghuazhen Fm). There may be two possibilities for the evolution of faults (Fig. 15C and D), i) Since the Pliocene (horizon T01), BZ8-4 structure began to be controlled by the NNW-SSE transtensional stress field of Neotectonism (Yu et al., 2011; Teng and ZouHao, 2014), a fault array consisting of six overlapping faults in plan view occurred at depth as blind faults, they subsequently reached free surface after radial propagation and switched from being blind to a syn-sedimentary growth mode. ii) These faults developed as blind faults during the deposition of Lower member of Minghuazhen Fm, the transtension of Neotectonism activated them, and their fault planes reached free surface and turned into syn-sedimentary overlapping faults. These faults are ①segment MA + Fa, ②segment AB + Fb, ③segment BC + Fc, ④segment CD + Fd, ⑤segment DE + Fe, and ⑥ segment EN. (Figs. 4 A, Fig. 15 C–D). Their subsequent lateral propagation and linkage formed the surface of Fault F1 in the Neogene strata. At the same time, the lateral lengthening of fault surface will inevitably lead to the increase of the fault height and result in the vertical linkage with previous fault surface in the Paleogene strata to form the unified Fault F1 (Watterson, 1986; Kim and Sanderson, 2005). Their right part of segments are degraded to the present branch faults in the hanging wall of Fault F1.

## 8. Discussion

### 8.1. Identification of lateral segmentation and linkage of normal faults along-strike

The growth and linkage of segmented normal faults is an important advance in the study of normal fault evolution in recent years. The identification of fault segments is the key to fault growth examination. This study particularly describes a variety of approaches for fault segment identification: i) Using 2D and 3D displacement patterns to identify the original segments prior to fault linkage. The displacement minima represent the boundary of the fault segments on D-d profiles, and the displacement contour patterns are used to reveal the segmentation characteristics of faults. Studies have presented anomalous displacement distribution surrounding branch or intersection lines, which displayed to be sub-vertical or sub-horizontal zones. ii) Identification of fault segments based on geometric characteristics of 3D fault surfaces. The distribution of dip angle and azimuth on the surface of Fault F1 clearly illustrates the 3D segmentation characteristics, which are typically characterized by lateral or vertical geometrical anomalies surrounding the branch or intersection lines.

Based on the above segmentation characteristics of faults, we have identified two types of fault interaction styles (Fig. 14): i) Fault intersection style. Faults F2 and Fa intersect Fault F1 at a large angle ca. 90° and 45° respectively during Paleogene, which result in the geometrical and displacement distribution anomalies surrounding intersection lines (intersection line A-A′ and C–C') on the Area A3 of Fault F1, but the geometry and displacement distribution of intersecting faults on both sides of the intersection line are not geometrically and kinematically correlated. The geometrical and kinematic characteristics of Faults F2 and Fa show that their lateral propagation is mechanically retarded by Fault F1. Therefore, the geometrical and displacement distribution anomalies surrounding intersection lines on the lower part of surface of Fault F1 (Area A3) are not the results of initial fault propagation, interaction and linkage, but caused by the intersection of faults with different strike. Here we call them fault intersection style, to distinguish it from the more widely discussed "propagation, interaction and linkage" of segments along fault strike. ii) Fault linkage style. For the overlapping faults as F1 fault network during Neogene, the lateral propagation, interaction and linkage of individual faults typically result in the formation of a unified fault, the linked fault exhibits the segmentation characteristics of geometry and kinematics and meanwhile, some part of fault segments are downgraded to branch faults in the hanging wall of master fault (Childs et al., 1993; Dawers and Underhill, 2000). We here called it fault linkage style (Figs. 14 A and Fig.15 D). Their geometry and displacement distribution on both sides of the branch line display high correlation, indicating that they were originally the same faults prior to segment linkage.

Therefore, attention must be paid to the interaction between faults in the examination of fault evolution, especially in the multiphase rift, multiphase extensions and the change of extension direction lead to the development and interaction of faults with different strikes. In this context, both of these fault interaction styles will occur. They are generally difficult to distinguish. If the examination is only based on their segmentation features, it may lead to wrong conclusions.

### 8.2. Identification of vertical segmentation and dip-linkage of normal faults

We have also described the geometric and kinematic segmentation characteristics of Fault F1 in dipping direction, and pointed out that fault zone F1 actually develops two sets of fault systems, the upper and the lower. Fault F1 is the result of dip-linkage of the upper and lower faults. The distribution pattern of fault displacement in the lower part is primarily parallel to the horizon traces, which represents the characteristics of syn-sedimentary faults. Whereas the upper fault system

displays the combination of elliptical and parallel displacement contour pattern, which reflects the evolution from blind faults to syn-sedimentary faults (Childs et al., 2003; Baudon and Cartwright, 2008c). The linkage zone of the upper and lower fault surfaces exhibits a significant reduction of displacement and dip angles, and presents as an anomaly zone distributed between horizon T3M and T2 on fault surface, and displays a tabular feature on the T-z plots. Especially, we discovered a new type of displacement pattern, the "negative ellipse of displacement contours", which can clearly indicate the dip-linkage zone of vertically segmented fault surfaces. Conventionally, this type of dip linkage is generally hard to be identified, because their relay structures are normally not resolved by the seismic data. Here, vertical segmentation can be identified based on quantitative analysis of geometry and kinematics on 3D fault surface.

In addition , fault shape is commonly controlled by dip linkage, or specifically, the lateral separation of dip segments (Fig. 9) (Rotevatn and Jackson, 2014; Delogkos et al., 2020). The dip linkage of upper and lower segment of Fault F1 produce a slight ramp-flat-ramp geometry, the zone of dip linkage actually corresponds to the flat, which is favorable to the formation of fault-bent folds. Actually, two overlapping, fault-parallel anticlines are developed adjacent to Fault F1 (Figs. 4 C, Fig.5). We infer that fault geometry may be responsible for the formation of the hanging-wall folds. These folds are normally favorable traps for oil and gas.

At present, the widely accepted fault growth models, wherever isolated or coherent growth model, they all focus on the lateral growth and linkage of faults and ignore the dip-linkage characteristics of faults and their influence on fault geometry and kinematics. By quantitative analysis of the 3D geometry and kinematics of the fault, we have restored the evolution process of fault zone F1 in three-dimension, revealed the interaction of multiphase faults in strike and dip oriented directions, and established the 3D evolution model of normal faults.

## 9. Conclusions

Integrating seismic interpretation with the 2D/3D geometry and displacement distribution of faults in the BZ8-4 structure, the WBS, BBB, demonstrates that the fault zone F1 experienced two stages of extension during the paleogene and Neogene. The present single continuous fault surface of Fault F1 was developed through the lateral and vertical growth and linkage of multiple fault surfaces. The Fault F1 is vertically coalesced by the upper and lower fault surfaces. The coalescence zone is characterized by an anomaly zone with reductions in dipping angle and displacement on the fault surface located between the horizon T3M and T2. The displacement anomaly zone is manifested as a series of ellipses centered the displacement minima. During each extensional stage, Fault F1 also shows segmentation characteristics along strike. The identification of fault segmentation is the vertical anomaly zone of geometry and displacement distribution locateded near the branch or interaection lines of interacting faults. The fault interaction style in rift stage is characterized by the intersection of faults with different strikes, i.e. fault intersection style. During Neogene, the interaction between faults is characterized by propagation, interaction and linkage of overlapping faults, i.e. fault linkage style. Whether the displacement distribution between the interaction faults shows a significant correlation on both sides of the intersection lines is the key to distinguish the two styles. The segmentation characteristics caused by fault intersections cannot be used as the mark of fault segment linkage. Thus correct differentiation of the fault interactions is vital for the examination of fault evolution.

The evolution of the fault zone F1 can be divided into the following distinct stages. i)The Paleogene faulting are initiated in the middle Eocene, with the development of the Fault F1, F2 and Fa of different strikes, and subsequent intersection between them during the deposition of the Shahejie Fm up to the Mbr 3 of the Dongying Fm. ii) These faults ceased to be active and became buried during the deposition of the Mbr 2 of the Dongying Fm. iii) During the Neogene, especially from the Neotectonic phase, an en-echlon fault array was developed above the faults in the rift stage. Their lateral propagation and linkage result in the dip linkage with the lower fault surfaces to form the present unified Fault F1.

The lateral and dip linkage of normal faults will provide insights into the timing of fault activity which has a direct application to hydrocarbon migration and accumulation associated with faults.

## Author statement

**Simin Sun:** Conceptualization, Methodology, Most of investigation, MS Writing and Editing;

**Huayao Zou**: Part of investigation, Original draft preparation.

**Chengmin Niu**: Seismic interpretation.

**Huaiqiang Ren**: Figures preparation.

## Declaration of Competing Interest

The authors declare that they have no known competing financial interests or personal relationships that could have appeared to influence the work reported in this paper.

## Data availability

The data that has been used is confidential.

## Acknowledgements

The authors are thankful for the constructive comments from Editor Ian Alsop, and anonymous reviewers. This work was supported by National Major Science and Technology Projects of China: [2016ZX05024-003-008]

## References

Anders, M.H., Schlische, R.W., 1994. Overlapping faults, intrabasin highs, and the growth of normal faults. J. Geol. 102, 165–180.

Barnett, J.A.M., Mortimer, J., Rippon, J.H., Walsh, J.J., Watterson, J., 1987. Displacement geometry in the volume containing a single normal fault. AAPG Bull. 71, 925–937.

Baudon, C., Cartwright, J., 2008a. The kinematics of reactivation of normal faults using high resolution throw mapping. J. Struct. Geol. 30, 1072–1084.

Baudon, C., Cartwright, J., 2008b. Early stage evolution of growth faults: 3D seismic insights from the Levant Basin, Eastern Mediterranean. J. Struct. Geol. 30, 888–898.

Baudon, C., Cartwright, J., 2008c. 3D seismic characterisation of an array of blind normal faults in the Levant Basin, Eastern Mediterranean. J. Struct. Geol. 30, 746–760.

Camanni, G., Roche, V., Childs, C., Manzocchi, T., et al., 2019. The three-dimensional geometry of relay zones within segmented normal faults. J. Struct. Geol. 129, 103895.

Cartwright, J.A., Trudgill, B.D., Mansfield, C.S., 1995. Fault growth by segment linkage: an explanation for scatter in maximum displacement and trace length data from the Canyonlands grabens of SE Utah. J. Struct. Geol. 17, 1319–1326.

Chapman, T.J., Meneilly, A.W., 1990. Fault displacement analysis in seismic exploration. First Break 8, 11–22.

Childs, C., Easton, S.J., Vendeville, B.C., Jackson, M.P.A., Lin, S.T., Walsh, J.J., Watterson, J., 1993. Kinematic analysis of faults in a physical model of growth faulting above a viscous salt analogue. Tectonophysics 228, 313–329.

Childs, C., Watterson, J., Walsh, J.J., 1995. Fault overlap zones within developing normal fault systems. J. Geol. Soc. London 152, 535–549.

Childs, C., Nicol, A., Walsh, J.J., Watterson, J., 1996. Growth of vertically segmented normal faults. J. Struct. Geol. 18, 1389–1397.

Childs, C., Nicol, A., Walsh, J.J., Watterson, J., 1996. Growth of vertically segmented normal faults. J. Struct. Geol. 18, 1389–1397.

Childs, C., Nicol, A., Walsh, J.J., Watterson, J., 2003. The growth and propagation of synsedimentary faults. J. Struct. Geol. 25, 633–648.

Cohneally, J., Childs, C., Walsh, J.J., 2014. Contrasting origins of breached relay zone geometries. J. Struct. Geol. 58, 59–68.

Collanega, L., Siuda, K., Christopher, A.L., Jackson, et al., 2019. Normal fault growth influenced by basement fabrics: the importance of preferential nucleation from pre-existing structures. Basin Res. 31 (4).

Cowie, P.A., Scholz, C.H., 1992. Displacement–length scaling relationship for faults: data synthesis and discussion. J. Struct. Geol. 14, 1149–1156.

Dawers, N.H., Underhill, J.R., 2000. The role of fault interaction and linkage in controlling syn-rift stratigraphic sequences: Statfjord East area, northern North Sea. AAPG (Am. Assoc. Pet. Geol.) Bull. 84, 45–64.
Dawers, N.H., Anders, .M.H., Scholz, C.H., 1993. Growth of normal faults: displacement-length scaling. Geology 21, 1107–1110.
Delogkos, E., Saqab, M.M., Walsh, J.J., Roche, V., Childs, C., 2020. Throw variations and strain partitioning associated with fault-bend folding along normal faults. Solid Earth 11, 935–945.
Deng, H., Mcclay, K., 2021. Three-dimensional Geometry and Growth of a Basement-Involved Fault Network Developed during Multiphase Extension, Enderby Terrace, NW Shelf of Australia, vol. 133. Geological Society of America Bulletin, pp. 9–10.
Deng, H., McClay, K., Bilal, A., 2020. 3D structure and evolution of an extensional fault network of the eastern Dampier Sub-basin, North West Shelf of Australia. J. Struct. Geol. 132, 103972.
Du, Q.X., Guo, S.B., Shen, X.L., Cao, Z.H., Zhang, X.L., Li, Y.S., 2016. Palaeo-water characteristics of the member 1 of paleogene Shahejie formation in southern Nanpu sag, Bohai Bay Basin. J. Palaeogeogr. 18, 173–183.
Duffy, O.B., Bell, R.E., Jackson, C.A., Gawthorpe, R.L., 2015. Fault growth and interactions in a multiphase rift fault network: Horda Platform, Norwegian North Sea. J. Struct. Geol. 80, 99–119.
Fan, W.M., Zhang, H.F., Baker, J., Jarvis, K.E., Mason, P.R.D., Menzies, M.A., 2000. On and off the North China craton: where is the Archaean keel? J. Petrol. 41, 933–950.
Ferrill, D.A., Stamatakos, A.J., Sims, D., 1999. Normal fault corrugation: implications for growth and seismicity of active normal faults. J. Struct. Geol. 21, 1027–1038.
Fossen, H., Rotevatn, A., 2016. Fault linkage and relay structures in extensional settings-A review. Earth Sci. Rev. 154, 14–28.
Frankowicz, E., McClay, K.R., 2010. Extensional fault segmentation and linkages, Bonaparte basin, outer North west Shelf, Australia. AAPG (Am. Assoc. Pet. Geol.) Bull. 94, 977–1010.
Ge, H.X., Anderson, J.K., 2007. fault throw profile and kinematics of normal fault: conceptual models and geologic examples. Geol. J. China Univ. 13, 75–88, 001.
Gong, Z.S., 2004. Late-stage fault activities and oil and gas reservoir formation of China's offshore basins (in Chinese). Petrol. Geol. 2, 12–19.
Gong, Z.S., Wang, G.C., 2001. Neotectonism and late hydrocarbon accumulation in Bohai sea (in Chinese). Acta Petrol. Sin. 22, 1–7.
Hao, F., Zhou, X.H., Zhu, Y.M., et al., 2011. Lacustrine source rock deposition in response to co-evolution of environments and organisms controlled by tectonic subsidence and climate, Bohai Bay Basin, China. Org. Geochem. 42, 323–339.
He, L., Wang, J., 2004. Tectono-thermal modeling of sedimentary basins with episodic extension and inversion: a case history of the Jiyang Basin. North China: Basin Res. 16, 587–599.
Henstra, G.A., Rotevatn, A., Gawthorpe, R.L., et al., 2015. Evolution of a major segmented normal fault during multiphase rifting: the origin of plan-view zigzag geometry. J. Struct. Geol. 74, 45–63.
Henza, A.A., Withjack, M.O., Schlische, R.W., 2011. How do the properties of a preexisting normal-fault population influence fault development during a subsequent phase of extension? J. Struct. Geol. 33, 1312–1324.
Hou, G.T., Qian, X.L., Cai, D.S., 2001. The tectonic evolution of Bohai basin in Mesozoic and cenozoic time. Acta Sci. Nauralium Univ. Pekin. 37 (6), 845–851.
Jackson, A.L., Rotevatn, A., 2013. 3D seismic analysis of the structure and evolution of a salt-influenced normal fault zone: a test of competing fault growth models. J. Struct. Geol. 54, 215–234.
Kattenhorn, S.A., Pollard, D.D., 2001. Integrating 3-D seismic data, field analogs, and mechanical models in the analysis of segmented normal faults in the Wytch Farm oil field, southern, England, United Kingdom. AAPG Bull. 85, 1183–1210.
Kim, Y.S., Sanderson, D.J., 2005. The relationship between displacement and length of faults: a review. Earth Sci. Rev. 68, 317–334.
Kiram, E.L., Tiercelin, J.J., Turdu, C.L., Andrew, S.C., Reynolds, D.J., Bernard, L.G., Scholz, C.A., 2002. Control of normal fault interaction on the distribution of major Neogene sedimentary depocenters, lake Tanganyika, East African rift. AAPG (Am. Assoc. Pet. Geol.) Bull. 86 (6), 1027–1059.
Kristensen, M.B., Childs, C.J., Korstgard, J.A., 2008. The 3D geometry of small-scale relay zones between normal faults in soft sediments[J]. J. Struct. Geol. 30, 257–272.
Li, S.Z., Suo, Y.H., Dai, L.M., et al., 2010. Development of the Bohai Bay Basin and destruction of the north China craton. Earth Sci. Front. 17, 064-089.
Li, S.Z., Zhao, G., Dai, L., et al., 2012. Cenozoic faulting of the Bohai Bay Basin and its bearing on the destruction of the eastern North China craton[J]. J. Asian Earth Sci. 47, 80–93.
Lohr, T., Krawczyk, C.M., Oncken, O., Tanner, D.C., 2008. Evolution of a fault surface from 3D attribute analysis and displacement measurements. J. Struct. Geol. 30, 690–700.
Maerten, L., Willemse, E.J.M., Pollard, D.D., Rawnsley, K., 1999. Slip distributions on intersecting normal faults. J. Struct. Geol. 21, 259–271.
Mansfield, C.S., Cartwright, J.A., 1996. High resolution fault displacement mapping from three-dimensional seismic data: evidence for dip linkage during fault growth. J. Struct. Geol. 18 (2/3), 249–263.
Mansfield, C., Cartwright, J., 2001. Fault growth by linkage; observations and implications from analogue models. J. Struct. Geol. 23, 745–763.
Marchal, D., Guiraud, M., Rives, T., 2003. Geometric and morphologic evolution of normal fault planes and traces from 2D to 4D. J. Struct. Geol. 25, 135–158.
Mcleod, A.E., Dawers, N.H., Underhill, J.R., 2000. The propagation and linkage of normal faults: insights from the Strathspey–Brent–Statfjord fault array, northern North Sea. Basin Res. 12, 263–284.
Meng, Q.R., Wu, G.L., Fan, L.G., Wei, H.H., 2019. Tectonic evolution of early Mesozoic sedimentary basins in the North China block. Earth Sci. Rev. 190, 416–438.
Morley, C.K., 2002. Evolution of large normal faults: evidence from seismic reflection data. AAPG (Am. Assoc. Pet. Geol.) Bull. 86, 961–978.
Morley, C.K., Nelson, R.A., Patton, T.L., Munn, S.G., 1990. Transfer zones in the East African rift system and their relevance to hydrocarbon exploration in rifts. AAPG (Am. Assoc. Pet. Geol.) Bull. 74, 1234–1253.
Morley, C.K., Haranya, C., Phoosongsee, W., et al., 2004. Activation of rift oblique and rift parallel pre-existing fabrics during extension and their effect on deformation style: examples from the rifts of Thailand[J]. J. Struct. Geol. 26 (10), 1803–1829.
Nicol, A., Watterson, J., Walsh, J.J., Childs, C., 1996. The shapes, major axis orientations and displacement patterns of fault surfaces. J. Struct. Geol. 18, 235–248.
Nixon, C.W., Sanderson, D.J., Dee, S.J., Bull, J.M., Humphreys, R.J., Swanson, M.H., 2014. Fault interactions and reactivation within a normal-fault network at Milne Point, Alaska. AAPG (Am. Assoc. Pet. Geol.) Bull. 98, 2081–2107.
Peacock, D.C.P., 2002. Propagation, interaction and linkage in normal fault systems. Earth Sci. Rev. 58, 121–142.
Peacock, D.C.P., Sanderson, D.J., 1991. Displacements, segment linkage and relay ramps in normal fault zones. J. Struct. Geol. 13, 721–733.
Peacock, D.C.P., Sanderson, D.J., 1994. Geometry and development of relay ramps in normal fault systems. AAPG (Am. Assoc. Pet. Geol.) Bull. 78, 147–165.
Peacock, D., Zhang, X., 1994. Field examples and numerical modelling of oversteps and bends along normal faults in cross-section. Tectonophysics 234, 147–167.
Peacock, D., Nixon, C.W., Rotevatn, A., Sanderson, D.J., Zuluaga, L.F., 2017. Interacting faults. J. Struct. Geol. 97, 1–22.
Phillips, T.B., Jackson, A.L., Bell, R.E., Duffy, O.B., Fossen, H., 2016. Reactivation of intrabasement structures during rifting: a case study from offshore southern Norway. J. Struct. Geol. 91, 54–73.
Phillips, T.B., Fazlikhani, H., Gawthorpe, R.L., Fossen, H., Jackson, C.A.-L., Bell, R.E., et al., 2019. The influence of structural inheritance and multiphase extension on rift development, the northern North Sea. Tectonics 38, 4099–4126.
Qi, J.F., Yang, Q., 2010. Cenozoic structural deformation and dynamic processes of the Bohai Bay basin province, China. Mar. Petrol. Geol. 27, 757–771.
Ren, J.Y., Tamaki, K., Li, S.T., Junxia, Z., 2002. Late Mesozoic and Cenozoic rifting and its dynamic setting in Eastern China and adjacent areas. Tectonophysics 344, 175–205.
Roche, V., Childs, C., Madritsch, H., Camanni, G., 2020. Layering and Structural Inheritance Controls on Fault Zone Structure in Three Dimensions: a Case Study from the Northern Molasse Basin, switzerland, vol. 177. Geological Society of London, pp. 493–508.
Roche, V., Camanni, G., Childs, C., Manzocchi, T., Walsh, J., et al., 2021. Variability in the three-dimensional geometry of segmented normal fault surfaces. Earth Sci. Rev. 11, 103523.
Rotevatn, A., Jackson, A.-L.C., 2014. 3D structure and evolution of folds during normal fault dip linkage. J. Geol. Soc. 171, 821–829. London.
Schlische, R.W., 1995. Geometry and origin of fault-related folds in extensional settings. Bull. AAPG 79, 1661–1678.
Schultz, R.A., Fossen, H., 2002. Displacement–length scaling in three-dimensions: the importance of aspect ratio and application to deformation bands. J. Struct. Geol. 24, 1389–1411.
Spahic, Darko, Grasemann, Bernhard, Exner, Ulrike, 2013. Identifying fault segments from 3D fault drag analysis (Vienna Basin, Austria). J. Struct. Geol. 55, 182–195.
Su, Jinbao, Zhu, Wenbin, Jia, Wei, et al., 2011. fault growth and linkage: implications for tectono-sedimentary evolution in the Chezhen basin of Bohai Bay, eastern China. AAPG (Am. Assoc. Pet. Geol.) Bull. 95, 1–26.
Sun, S.M., Ji, H.C., Wang, J.W., et al., 2016. Segmentation characteristics and evolution of Xinanzhuang Fault in Nanpu sag, Bohai Bay Basin. Petrol. Geol. Exp. 38, 628–634.
Suo, Y.H., Li, S.Z., Liu, X., et al., 2013. Structural characteristics of NWW-trending active fault zones in East China: a case study of the Zhangjiakou-Penglai Fault Zone. Acta Petrol. Sin. 29, 953–966.
Teng, C.Y., Zou, H.Y., Hao, F., 2014. Control of differential tectonic evolution on petroleum occurrence in Bohai Bay Basin. Sci. China Earth Sci. 57, 1117–1128.
Teng, C.Y., Hao, F., Zou, H.Y., Zhou, X.H., Xu, C.G., 2016. Tan-Lu fault system and its significance in oil accumulation in the central Liaodong Bay subbasin, Bohai Bay Basin, China. AAPG Bull. 100, 289–314.
Torabi, A., Alaei, B., Libak, A., 2019. Normal fault 3D geometry and displacement revisited: insights from faults in the Norwegian Barents Sea. Mar. Petrol. Geol. 99, 135–155.
Trudgill, B., Cartwright, J., 1994. Relay-ramp forms and normal-fault linkages, Canyonlands National Park, Utah. Geol. Soc. Am. Bull. 106, 1143–1157.
Vergely, P., Hou, M.J., Wang, Y.M., et al., 2007. The kinematics of the Tan-Lu Fault zone during the Mesozoic-Palaeocene and its relations with the North China-South China block collision. Bull. Soc. Geol. Fr. 178, 353–365.
Walsh, J.J., Watterson, J., 1987. Distributions of cumulative displacement and seismic slip on a single normal fault surface. J. Struct. Geol. 9 (8), 1039–1046.
Walsh, J.J., Watterson, J., Bailey, W.R., Childs, C., 1999. Fault relays, bends and branch-lines. J. Struct. Geol. 21, 1019–1026.
Walsh, J.J., Nicol, A., Childs, C., 2002. An alternative model for the growth of faults. J. Struct. Geol. 24, 1669–1675.
Walsh, J.J., Bailey, W.R., Childs, Nicol C.A., Bonson, C.G., 2003. Formation of segmented normal faults: a 3-D perspective. J. Struct. Geol. 25, 1251–1262.
Wang, G.M., Xiong, Z.H., Zhang, J., 2017. Characterization of Fault system and its control on reservoirs in the Bozhong sag, Bohai Bay Basin. Oil Gas Geol. 38 (1), 62–70.
Watterson, J., 1986. Fault dimensions, displacements and growth[J]. Pure Appl. Geophys. 124 (1), 365–373.
Watterson, J., Nicol, A., Walsh, J.J., et al., 1998. Strains at the intersections of synchronous conjugate normal faults. J. Struct. Geol. 20 (4), 363–370.

Willemse, E.J.M., 1997. Segmented normal faults: correspondence between three-dimensional mechanical models and field data. J. Geophys. Res. 102, 675–692.
Xu, J., Niu, J.Y., Lü, Y.J., et al., 2009. Neotectonics and neotectonic activities of Yingkou-Weifang fault zone (in Chinese). Acta Petrol. Sin. 30, 498–505.
Xu, S., Hao, F., Xu, C., et al., 2014. Tracing migration pathways by integrated geological, geophysical, and geochemical data: a case study from the JX1-1 oil field, Bohai Bay Basin, China[J]. AAPG (Am. Assoc. Pet. Geol.) Bull. 98 (10), 2109–2129.
Xu, C.Q., Zhang, Z., Zhang, X.T., Guo, R., Zhang, Z.Q., 2018. Tectonic evolution and hydrocarbon model of western Bohai sea. J. Northeast Petrol. Univ. 42 (1), 68–77.
Yu, Y.X., Zhou, X.H., Xu, C.G., et al., 2011. Characteristics and formation mechanisms of the Cenozoic faults in the Bohai Sea waters (in Chinese). Oil Gas Geol. 32, 273–279.
Zhai, M.G., Peng, P., 2007. Paleoproterozoic events in the North China craton. Acta Petrol. Sin. 23, 2665–2682.
Zhang, X.Q., Wu, Z.P., Zhou, X.H., et al., 2017. Cenozoic tectonic characteristics and evolution of the southern Bohai sea. Geotect. Metallogenia 41, 50–60. https://doi.org/10.16539/j.ddgzyckx.2017.01.004.
Zhang, Z., Xu, C.Q., Zhang, Z.Q., et al., 2018. Evolution characteristics and their controlling actions on the hydrocarbon accumulation for the faults in Western sag of Bozhong. Pet. Geol. Oilfield Dev. Daqing 37 (1), 9–14.
Zhu, G., Liu, G.S., Niu, M.L., et al., 2003. Transcurrent movement and genesis of the Tan-Lu fault zone (in Chinese). Geol. Bull. China 22, 200–207.